

Decomposing Global Feature Effects Based on Feature Interactions

Julia Herbinger

JULIA.HERBINGER@STAT.UNI-MUENCHEN.DE

Bernd Bischl

BERND.BISCHL@STAT.UNI-MUENCHEN.DE

Giuseppe Casalicchio

GIUSEPPE.CASALICCHIO@STAT.UNI-MUENCHEN.DE

Department of Statistics, LMU Munich

Munich Center for Machine Learning (MCML)

Editor:

Abstract

Global feature effect methods, such as partial dependence plots, provide an intelligible visualization of the expected marginal feature effect. However, such global feature effect methods can be misleading, as they do not represent local feature effects of single observations well when feature interactions are present. We formally introduce *generalized additive decomposition of global effects* (GADGET), which is a new framework based on recursive partitioning to find interpretable regions in the feature space such that the interaction-related heterogeneity of local feature effects is minimized. We provide a mathematical foundation of the framework and show that it is applicable to the most popular methods to visualize marginal feature effects, namely partial dependence, accumulated local effects, and Shapley additive explanations (SHAP) dependence. Furthermore, we introduce a new permutation-based interaction test to detect significant feature interactions that is applicable to any feature effect method that fits into our proposed framework. We empirically evaluate the theoretical characteristics of the proposed methods based on various feature effect methods in different experimental settings. Moreover, we apply our introduced methodology to two real-world examples to showcase their usefulness.

Keywords: interpretable machine learning, feature interactions, partial dependence, accumulated local effect, SHAP dependence

1 Introduction

Machine learning (ML) models are increasingly used in various application fields—such as medicine (Shipp et al., 2002) or social sciences (Stachl et al., 2020)—due to their better predictive performance compared to simpler, inherently interpretable models. The superior performance often comes from complex non-linear relationships or feature interactions in the data which can be modeled more accurately by more flexible and complex ML models. However, the more complex and flexible a model, the harder it becomes to explain its inner workings. A lack of explainability might hurt trust or might even be a deal-breaker for high-stakes decisions (Lipton, 2018). Hence, ongoing research on model-agnostic interpretation methods to explain any ML model has grown quickly in recent years.

One promising type of explanation is produced by feature effect methods which explain how features influence the model predictions (similarly to the coefficients in a linear model) (Molnar, 2022). We distinguish between local and global feature effect methods. Local

feature effect methods—such as individual conditional expectation (ICE) curves (Goldstein et al., 2015) or Shapley values / Shapley additive explanations (SHAP) (Štrumbelj and Kononenko, 2014; Lundberg and Lee, 2017)—explain how each feature influences the prediction of a single observation. In contrast, global feature effect methods explain the general model behavior based on the given data. Since global feature effects of ML models are often non-linear, it is easier to visualize them as done by partial dependence (PD) plots (Friedman, 2001), accumulated local effects (ALE) plots (Apley and Zhu, 2020), or SHAP dependence (SD) plots (Lundberg et al., 2019).

Aggregating individual explanations to a global explanation (e.g., ICE to PD curves) has the advantage that the global feature effects can be presented in an easy-to-understand way. However, the aggregation step might cause information loss due to heterogeneity in local effects (e.g., see the different shapes of ICE curves in Figure 1). This so-called aggregation bias is usually induced by feature interactions leading to a global feature effect that is not representative for many individuals in the data (Herbinger et al., 2022; Mehrabi et al., 2021). We term this heterogeneity *interaction-related heterogeneity*. Therefore, global explanations might be misleading or not give a complete picture when feature interactions are present, as illustrated in the bikesharing example in Figure 1 (see also Section 7). This

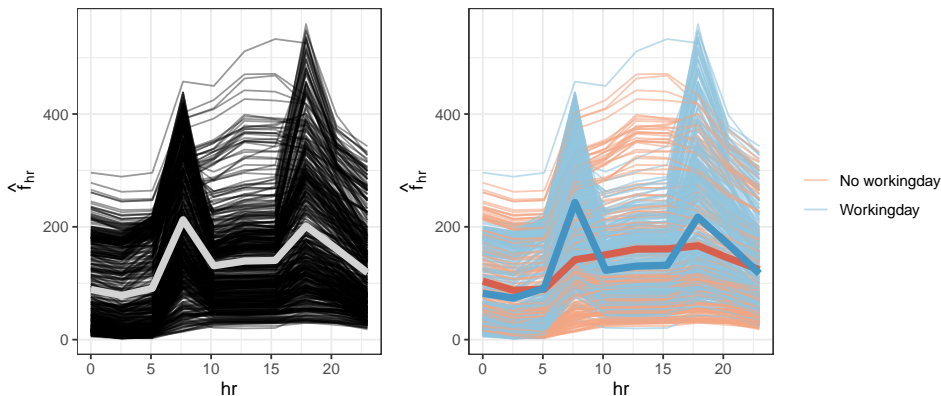


Figure 1: Left: ICE and global PD curves of feature hr (hour of the day) of the bikesharing data set (James et al., 2022). Right: ICE and regional PD curves of hr depending on feature $workingday$. The feature effect of hr on predicted bike rentals is different on working days compared to non-working days, which is due to aggregation not visible in the global feature effect plot (left).

is particularly relevant when ML models are trained on biased data (Mehrabi et al., 2021). The ML model might learn this bias, which might not be visible in global explanations due to aggregation (e.g., see COMPAS example in Section 7).

To bridge the gap between local and global effect explanations, so-called subgroup approaches that partition the feature space to obtain meaningful regional explanations within each partition have recently been introduced (e.g., Hu et al., 2020; Molnar et al., 2023; Scholbeck et al., 2022; Herbinger et al., 2022). Herbinger et al. (2022) introduced a recursive partitioning algorithm that finds interpretable subgroups in the data where the feature

interactions between a specific feature of interest and other features are minimized based on ICE curves. Thus, the resulting regional PD plots of the feature of interest are more representative for the individuals within the respective subgroup. However, the method is limited to PD plots with one feature of interest and, hence, leads to different partitions if multiple features of interest are considered. The mathematical foundation of their method relies on the functional ANOVA decomposition (Stone, 1994; Hooker, 2007) of the prediction function. Being able to decompose the predictions into main and higher-order effects is very appealing to better understand how features individually and jointly influence the predictions. However, the decomposition might not be unique and the respective estimation complex in the presence of feature interactions (Hooker, 2007; Lengerich et al., 2020).

Contributions. We introduce the framework GADGET, which partitions the feature space into interpretable subspaces by minimizing feature interactions based on some feature effect method. We prove that the objective of GADGET minimizes feature interactions of any feature subset and for any feature effect method that satisfies the *local decomposability* axiom (Section 4.1 and 4.2). We show that the most popular feature effect methods (PD, ALE, and SD) satisfy the *local decomposability* axiom. For each method, we introduce an estimation and visualization technique for the regional feature effect and the interaction-related heterogeneity (Section 4.3-4.5). Moreover, we propose several measures to quantify feature interactions based on GADGET, which provide more insights into the learned effects and remaining interaction-related heterogeneity (Section 4.6). To the best of our knowledge, we are the first who introduce such a flexible framework for more insights into regional feature effects and feature interactions. Additionally, we introduce the permutation interaction test (PINT) algorithm to detect significant feature interactions based on the underlying feature effect method (Section 5). Finally, we empirically evaluate the theoretical characteristics of the different methods based on several simulation settings (Section 6).

Open Science and Reproducibility. The implementation of the proposed methods as well as reproducible scripts for the experiments are provided in Online Appendix 1.

2 Background and Related Work

In this section, we introduce relevant notation and summarize related work as well as the required methodological background for this paper.

2.1 General Notation

We consider a feature space $\mathcal{X} \in \mathbb{R}^p$ and a target space \mathcal{Y} that for instance, in the case of regression is $\mathcal{Y} = \mathbb{R}$. The random variables for the features are denoted by $X = (X_1, \dots, X_p)$ and Y for the target variable. The realizations of these random variables are sampled i.i.d. from the joint probability distribution $P_{X,Y}$ (which is unknown) and are denoted by $\mathcal{D} = \{(\mathbf{x}^{(i)}, y^{(i)})\}_{i=1}^n$. The i -th observation of \mathcal{D} is denoted by $\mathbf{x}^{(i)} = (x_1^{(i)}, \dots, x_p^{(i)})^T$ and the j -th feature by $\mathbf{x}_j = (x_j^{(1)}, \dots, x_j^{(n)})^T$. A true function f maps the feature space to the target space $f : \mathcal{X} \rightarrow \mathcal{Y}$. In ML, we strive to approximate this true relationship by a

prediction model \hat{f} , which is learned on \mathcal{D} . Furthermore, we denote $-j = \{1, \dots, p\} \setminus j$ to be the set of all features besides feature j .

2.2 Functional ANOVA Decomposition

The functional ANOVA decomposition has already been studied by Stone (1994) to explain prediction models. Hooker (2004, 2007), Rahman (2014), and Li and Rabitz (2012) (amongst others) generalized the approach, suggested further estimation algorithms, and provided several analyses with regard to decomposing an ML prediction function into so-called main and higher-order (interaction) effects. If the influence of the feature \mathbf{x}_j on the prediction function cannot solely be described by the main effect of \mathbf{x}_j because the prediction changes depending on another feature \mathbf{x}_k , then the prediction function exhibits an interaction between the features \mathbf{x}_j and \mathbf{x}_k . More formally, Friedman and Popescu (2008) defined the presence of an interaction between two features \mathbf{x}_j and \mathbf{x}_k by $\mathbb{E} \left[\frac{\delta^2 \hat{f}(X)}{\delta X_j \delta X_k} \right]^2 > 0$. If the feature \mathbf{x}_j does not interact with any other feature in \mathbf{x}_{-j} , the prediction function $\hat{f}(\mathbf{x})$ can be additively decomposed into a function $h_j(\mathbf{x}_j)$ that only depends on feature \mathbf{x}_j and another function $h_{-j}(\mathbf{x}_{-j})$ that only depends on all other features \mathbf{x}_{-j} , i.e., $\hat{f}(\mathbf{x}) = h_j(\mathbf{x}_j) + h_{-j}(\mathbf{x}_{-j})$.

The prediction function $\hat{f}(\mathbf{x})$ (if it is square-integrable) can be decomposed by using the functional ANOVA decomposition as follows:

$$\hat{f}(\mathbf{x}) = g_0 + \sum_{j=1}^p g_j(\mathbf{x}_j) + \sum_{j \neq k} g_{jk}(\mathbf{x}_j, \mathbf{x}_k) + \dots + g_{12\dots p}(\mathbf{x}) = \sum_{k=1}^p \sum_{\substack{W \subseteq \{1, \dots, p\}, \\ |W|=k}} g_W(\mathbf{x}_W), \quad (1)$$

where g_0 represents a constant, $g_j(\mathbf{x}_j)$ denotes the main effect of the j -th feature, $g_{jk}(\mathbf{x}_j, \mathbf{x}_k)$ is the pure two-way interaction effect between features \mathbf{x}_j and \mathbf{x}_k , and so forth. The last component $g_{12\dots p}(\mathbf{x})$ contains the residual term, which always allows for an exact decomposition.

We will now introduce the standard functional ANOVA decomposition and a generalization of it that is more suitable in the context of correlated features.

Standard Functional ANOVA Decomposition. The standard functional ANOVA decomposition (Hooker, 2004; Rahman, 2014) assumes that all features are independent. Hence, the joint probability density function $w(\mathbf{x})$ can be written as a product-type probability measure $w(\mathbf{x}) = \prod_{j=1}^p w_j(\mathbf{x}_j)$, with $w_j : \mathbb{R} \rightarrow \mathbb{R}_0^+$ being the marginal probability density function of the j -th feature. In this case, the component functions $g_W(\mathbf{x}_W)$ can be optimally and uniquely defined for a fixed prediction function $\hat{f}(\mathbf{x})$ if the *vanishing condition* is satisfied. The *vanishing condition* is given by $\int g_W(\mathbf{x}_W) w_j(\mathbf{x}_j) d\mathbf{x}_j = 0 \forall j \in W \neq \emptyset$, with $w_j(\mathbf{x}_j) \geq 0$ and $\int_{\mathbb{R}} w_j(\mathbf{x}_j) d\mathbf{x}_j = 1$ (see, e.g., Li and Rabitz, 2012; Rahman, 2014, for a detailed definition¹). Following from that, the component functions can be determined sequentially by

$$g_W(\mathbf{x}_W) = \int_{\mathbf{x}_{-W}} \left(\hat{f}(\mathbf{x}) w(\mathbf{x}) - \sum_{V \subset W} g_V(\mathbf{x}_V) \right) d\mathbf{x}_{-W}. \quad (2)$$

1. In Rahman (2014) this is called the strong annihilating condition.

Generalized Functional ANOVA Decomposition. When features are not independent from each other, the *vanishing condition* does not hold. Therefore, Hooker (2007) introduces a relaxed version of the *vanishing condition*² that leads to a unique decomposition of $\hat{f}(\mathbf{x})$, which they call the weighted functional ANOVA. The functional components cannot be determined sequentially (as in Eq. 2) and must be determined by solving a computationally more expensive optimization problem.

Thus, it is possible to decompose the prediction function in many different (valid) ways, with differing interpretations in the presence of feature interactions. Functional ANOVA decomposition is one possibility, which always leads to a unique decomposition. Hence, recent research has focused either on proposing models that directly include the respective conditions in the optimization process by constraints (e.g., Sun et al., 2022) or on purifying the resulting decomposition for specific models within the modelling process (e.g., Lengerich et al., 2020; Hu et al., 2022). While these approaches are first steps for computing the generalized functional ANOVA decomposition more efficiently, estimating the true underlying data distribution remains an open challenge that also influences the decomposition itself (Lengerich et al., 2020). First attempts in this direction have been proposed, for example by Sun et al. (2022) using an adaptive kernel method. Note that the estimation of the generalized functional ANOVA decomposition is only complex in the presence of feature interactions, otherwise the prediction function can easily and uniquely be decomposed into the main effects of each feature—e.g., estimated by a generalized additive model (GAM).

2.3 Visualizing Feature Effects

The visualization of feature effects provides a better understanding of how features individually or jointly influence the predicted outcome of an ML model. In this section, we introduce some of the most important global feature effect methods and relate them to the functional ANOVA decomposition.

Partial Dependence. The *PD plot* introduced by Friedman (2001) visualizes the marginal effect of a set of features $W \subset \{1, \dots, p\}$ by integrating over the joint distribution over all other features in $-W = \{1, \dots, p\} \setminus W$, which we denote by $\mathbb{P}(\mathbf{x}_{-W})$. Therefore, the PD function is defined by

$$f_W^{PD}(\mathbf{x}_W) = E_{X_{-W}}[\hat{f}(\mathbf{x}_W, X_{-W})] = \int \hat{f}(\mathbf{x}_W, \mathbf{x}_{-W}) d\mathbb{P}(\mathbf{x}_{-W}). \quad (3)$$

As the joint distribution $\mathbb{P}(\mathbf{x}_{-W})$ is usually unknown, the PD function is estimated using Monte-Carlo integration by $\hat{f}_W^{PD}(\mathbf{x}_W) = \frac{1}{n} \sum_{i=1}^n \hat{f}(\mathbf{x}_W, \mathbf{x}_{-W}^{(i)})$. Since the PD function is usually estimated for visualization purposes, the number of features in W is chosen to be one or two, and is visualized by the pairs $\{(\mathbf{x}_W^{(k)}, \hat{f}_W^{PD}(\mathbf{x}_W^{(k)}))\}_{k=1}^m$ for m grid points³.

The PD curve for $|W| = 1$ averages over heterogeneous effects that are induced by feature interactions between the feature \mathbf{x}_W and other features. These heterogeneous effects can be visualized using *ICE plots* (Goldstein et al., 2015), which measure the extent to which the

2. The relaxed vanishing condition is given by $\int_{\mathbb{R}} g_W(\mathbf{x}_W) w_W(\mathbf{x}_W) d\mathbf{x}_j = 0$ for $j \in W \neq \emptyset$, with $w(\mathbf{x})$ being a general probability density.

3. Instead of using all feature values \mathbf{x}_W , an equidistant grid or a grid based on randomly selected feature values or quantiles of \mathbf{x}_W are commonly chosen (Molnar et al., 2022).

prediction of each observation changes when the value of feature \mathbf{x}_W changes. Thus, ICE plots visualize each individual curve $\{(\mathbf{x}_W^{(k)}, \hat{f}(\mathbf{x}_W^{(k)}, \mathbf{x}_{-W}^{(i)}))\}_{k=1}^m$ for all $i \in \{1, \dots, n\}$, with the PD curve being the average over all ICE curves (see Figure 2).

While ICE plots can help to spot interactions between the feature of interest and other features by visual inspection, they do not reveal with which other features \mathbf{x}_W interacts and in which way these interactions influence the marginal effect of the feature of interest. To that end, Inglis et al. (2022) suggest different visualization techniques—such as Zenplots—that only show relevant 2-dimensional PD plots in a user-friendly layout. Other works focus on grouping ICE curves with similar shapes to find regions within the feature space where the regional PD plot can be interpreted reliably. For example, Britton (2019) suggests using an unsupervised clustering approach to group ICE curves based on their partial derivatives. A similar approach has been introduced by Zhang et al. (2021). However, Herbinger et al. (2022) showed that this approach can produce misleading interpretations and suggest a supervised approach to find interpretable regions where feature interactions are minimized and resulting regional PD estimates are more representative for the underlying observations.

Friedman (2001) argues that using PD functions as additive components in a functional decomposition can recover the prediction function up to a constant. Thus, the prediction function can be decomposed into an intercept g_0 and the sum of mean-centered PD functions with the same sequential procedure, as done for the standard functional ANOVA decomposition where lower-order effects are subtracted:

$$\hat{f}(\mathbf{x}) = g_0 + \sum_{k=1}^p \sum_{\substack{W \subseteq \{1, \dots, p\}, \\ |W|=k}} \left(\hat{f}_W^{PD,c}(\mathbf{x}_W) - \sum_{V \subset W} \hat{f}_V^{PD,c}(\mathbf{x}_V) \right), \quad (4)$$

with $\hat{f}_W^{PD,c}(\mathbf{x}_W) = \hat{f}_W^{PD}(\mathbf{x}_W) - \frac{1}{m} \sum_{k=1}^m \hat{f}_W^{PD}(\mathbf{x}_W^{(k)})$. Tan et al. (2018) furthermore note that if the prediction function can be written as a sum of main effects, it can be exactly decomposed by an intercept plus the sum of all mean-centered 1-dimensional PD functions.

Similar to standard functional ANOVA, Hooker (2007) illustrate that the decomposition via PD functions is misleading when features are highly correlated due to placing too much weight in sparse regions, which causes extrapolation.

Extrapolation Problem and ALE. Since the marginal distribution is used in PD functions, we *extrapolate* in empty or sparse regions of the feature space that might even be unrealistic (e.g., predicting a disease status for a pregnant man) when features are highly correlated. This can lead to inaccurate PD estimates, especially in the case of non-parametric models such as neural networks (Apley and Zhu, 2020).

Rather than integrating over marginal distributions (see Eq. 3), one possible solution to this challenge is to integrate over conditional distributions, which is known as a marginal (M) plot (Friedman, 2001). However, the M plot of feature \mathbf{x}_j not only represents the feature effect of the feature itself, but also includes the partial effects of features correlated with the feature of interest (see Appendix A for an example). Therefore, we cannot additively decompose the prediction function into individual M plot components, as done for PD in Eq. (4)⁴. As we focus on methods that allow an additive decomposition of the prediction

4. This is only possible if all features are independent of each other. The M plot then results in the PD plot, since the conditional joint distribution is then equivalent to the marginal joint distribution.

function and the isolated interpretation of individual feature effects, we will not cover M plots (i.e., conditional PD plots) in greater detail here.

ALE plots are based on conditional expectations and thus avoid extrapolation. However, they solely reflect the influence of the feature of interest on the predictions (Apley and Zhu, 2020). The uncentered ALE $f_W^{ALE}(x)$ for $|W| = 1$ at feature value $x \sim \mathbb{P}(\mathbf{x}_W)$ and with $z_0 = \min(\mathbf{x}_W)$ is defined by

$$f_W^{ALE}(x) = \int_{z_0}^x \mathbb{E} \left[\frac{\partial \hat{f}(X)}{\partial X_W} \middle| X_W = z_W \right] dz_W = \int_{z_0}^x \int \frac{\partial \hat{f}(z_W, \mathbf{x}_{-W})}{\partial z_W} d\mathbb{P}(\mathbf{x}_{-W} | z_W) dz_W. \quad (5)$$

ALE first calculates the local derivatives that are weighted by the conditional distribution $\mathbb{P}(\mathbf{x}_{-W} | z_W)$ and then accumulates the local effects to generate a global effect curve.

Eq. (5) is usually estimated by splitting the value range of \mathbf{x}_W in intervals and calculating the partial derivatives for all observations within each interval. The partial derivatives are estimated by the differences between the predictions of the upper ($z_{k,W}$) and lower ($z_{k-1,W}$) bounds of the k -th interval for each observation. The accumulated effect up to observation x is then calculated by summing up the average partial derivatives (weighted by the number of observations $n(k)$ within each interval) over all intervals until the interval that includes observation x , which is denoted by $k(x)$:

$$\hat{f}_W^{ALE}(x) = \sum_{k=1}^{k(x)} \frac{1}{n(k)} \sum_{i: \mathbf{x}_W^{(i)} \in]z_{k-1,W}, z_{k,W}] } \left[\hat{f}(z_{k,W}, \mathbf{x}_{-W}^{(i)}) - \hat{f}(z_{k-1,W}, \mathbf{x}_{-W}^{(i)}) \right]. \quad (6)$$

For interpretability reasons, ALE curves are usually centered by the average of the uncentered ALE curve to obtain $f_W^{ALE,c}(x) = \hat{f}_W^{ALE}(x) - \int f_W^{ALE}(\mathbf{x}_W) d\mathbb{P}(\mathbf{x}_W)$.

Another advantage of ALE is that they are computationally less expensive than PD functions. Compared to M plots, ALE also satisfies the additive recovery⁵. Note that Apley and Zhu (2020) defined the W -th order ALE function by the pure W -th order (interaction) effect, as done similarly for the functional ANOVA decomposition in Eq.(1). Furthermore, Apley and Zhu (2020) show that the ALE decomposition has an orthogonality-like property, which guarantees (similar to the generalized functional ANOVA) that the following decomposition is unique:

$$\hat{f}(\mathbf{x}) = g_0 + \sum_{\substack{W \subseteq \{1, \dots, p\}, \\ |W|=k}} \hat{f}_W^{ALE,c}(\mathbf{x}_W). \quad (7)$$

For details on estimating higher-order ALE functions, we refer to Apley and Zhu (2020).

The choice of a feature effect method will typically depend on the underlying research question. Generally, one distinguishes between understanding the model behavior or understanding the data-generating process. While PD generally answers the first question, ALE is more focused on answering the second question.

5. Meaning, the prediction function can be additively decomposed into main and higher-order effects by ALE functions (such as PD functions), as defined in Eq. (7).

SHAP Dependence. Another method that quantifies feature effects on a local level are Shapley values which have been transferred from game theory to an ML context (Shapley, 1953; Štrumbelj and Kononenko, 2014). The general idea behind this method is to distribute the payout of a single prediction of an ML model fairly among all features.

The Shapley value of a feature is then defined by the fair contribution of this feature to the prediction. Furthermore, Herren and Hahn (2022) showed that the Shapley value of feature \mathbf{x}_j at feature value $x_j = \mathbf{x}_j^{(i)}$ can be decomposed according to the functional ANOVA decomposition into main and interaction effects⁶:

$$\begin{aligned} \phi_j^{(i)}(x_j) &= \sum_{k=0}^{p-1} \frac{1}{k+1} \sum_{\substack{W \subseteq -j: \\ |W|=k}} \left(\mathbb{E}[\hat{f}(x_j, X_{-j}) | X_W = \mathbf{x}_W^{(i)}] - \sum_{V \subseteq \{W \cup j\}} \mathbb{E}[\hat{f}(X) | X_V = \mathbf{x}_V^{(i)}] \right) \\ &= g_j^c(x_j) + \sum_{k=1}^{p-1} \frac{1}{k+1} \sum_{W \subseteq -j: |W|=k} g_{W \cup j}^c(x_j, \mathbf{x}_W^{(i)}). \end{aligned} \quad (8)$$

While Shapley values only quantify the local effect of a feature on the prediction, Lundberg et al. (2019) propose the SHAP dependence (SD) plot as an alternative to PD plots. SD plots show the global behavior by visualizing the local Shapley values for all or a sample of observations of one feature, similarly to an ICE plot (see Figure 5). Thus, feature interactions between the feature of interest and other features also influence the shape of the resulting point cloud. Lundberg et al. (2019) suggest coloring the points according to another (potentially) interacting feature. However, if feature effects are very heterogeneous due to feature interactions, it might not be possible to identify a clear trend of the marginal feature effect (as observed similarly for ICE plots).

As with PD plots, M plots, or ALE plots, the means of estimating the conditional expectation for Shapley values is an ongoing discussion in current research (see, e.g., Sundararajan and Najmi, 2020; Chen et al., 2020). The approach taken might also influence the SD plot, since the estimation of Shapley values can generally be based on either marginal sampling (i.e., an interventional approach, similar to PD plots) or conditional sampling (i.e., an observational approach, similar to M plots). While the interventional approach also bears the problem of extrapolation, the observational approach requires the estimation of the conditional data distribution, which is still a challenging task (Aas et al., 2021). Chen et al. (2020) argue that the interventional approach is not generally wrong and can be useful if we want to derive explanations that are true to the model, while the observational approach should be used when we want to extract interpretations that are true to the data.

2.4 Quantification of Interaction Effects

Visualizing feature effects is a powerful technique to obtain a better understanding of how features influence the prediction function. However, useful visualizations are usually limited to a maximum of two features. Hence, to better comprehend which feature effects might depend on other features due to interactions, we are interested in detecting and quantifying the strength of feature interactions.

6. Similar decompositions and their estimation have been introduced in Hiabu et al. (2023) and Bordt and von Luxburg (2023).

Based on the definition of feature interactions in Section 2.2 and on the PD function, Friedman and Popescu (2008) introduced the H-Statistic as a global interaction measure between subsets of features. To quantify the interaction strength between a feature of interest \mathbf{x}_j and all other features \mathbf{x}_{-j} , the H-Statistic is calculated by

$$\hat{\mathcal{H}}_j^2 = \frac{\sum_{i=1}^n (\hat{f}^c(\mathbf{x}^{(i)}) - \hat{f}_j^{PD,c}(\mathbf{x}_j^{(i)}) - \hat{f}_{-j}^{PD,c}(\mathbf{x}_{-j}^{(i)}))^2}{\sum_{i=1}^n (\hat{f}^c(\mathbf{x}^{(i)}))^2}. \quad (9)$$

Hence, $\hat{\mathcal{H}}_j^2$ quantifies how much of the prediction function’s variance⁷ can be attributed to the interaction between feature \mathbf{x}_j and all other features \mathbf{x}_{-j} ⁸. Eq. (9) can be adjusted to quantify interactions of different order, such as two-way interactions (see Friedman and Popescu, 2008). Other global interaction measures to quantify two-way interactions based on PDs or SHAP interaction values have been suggested by Greenwell et al. (2018) and Herbringer et al. (2022). While these methods focus on detecting and quantifying two-way feature interactions, Hooker (2004) suggests an algorithm based on the idea of functional ANOVA decomposition to detect all important higher-order terms and visualizes the feature relationships in a network graph. However, the feature interactions are not quantified and thus cannot be ranked according to their influence on the prediction.

Next to global interaction measures, there exist multiple local interaction measures that quantify feature interactions for a single observation (e.g., Lundberg et al., 2019; Tsai et al., 2023; Blücher et al., 2022; Kumar et al., 2021).

3 Motivation: REPID and its Limitations

To obtain a better understanding of how features globally affect the predictions in the presence of feature interactions, Herbringer et al. (2022) propose the REPID method, which decomposes the global PD into regional PDs such that individual effects (ICE curves) are more homogeneous within each region. This section provides a short explanation of the REPID method and illustrates its limitations, which are addressed by our new framework introduced in Section 4.

The REPID method is based on a recursive partitioning algorithm (similar to CART by Breiman et al., 1984) that splits each parent node into two child nodes until a stop criterion is met. Compared to a common decision tree, the inputs are not the observations \mathbf{x} themselves, but the ICE curves belonging to the observations of one feature of interest \mathbf{x}_j . Herbringer et al. (2022) showed that their chosen objective minimizes interaction effects between the feature of interest and all other features. Therefore, the reduction at each split quantifies the interaction strength between the feature of interest and the feature used for splitting. Thus, the method provides more representative PD estimates in interpretable regions for a feature of interest as well as a ranking of considered two-way feature interactions.

For illustration purposes, consider the following simulation example that is often used in a slightly modified form in the context of feature interactions (see e.g., Goldstein et al.,

7. The denominator of Eq. (9) represents the prediction function’s variance, where $\hat{f}^c(\mathbf{x}^{(i)}) = \hat{f}(\mathbf{x}^{(i)}) - \frac{1}{n} \sum_{i=1}^n \hat{f}(\mathbf{x}^{(i)})$.

8. If the feature \mathbf{x}_j does not interact with any other feature in \mathbf{x}_{-j} , then the mean-centered joint effect function can be additively decomposed into: $f^c(\mathbf{x}) = f_j^{PD,c}(\mathbf{x}_j) + f_{-j}^{PD,c}(\mathbf{x}_{-j})$, leading to $\hat{\mathcal{H}}_j^2 = 0$.

2015; Herbinger et al., 2022): Let $X_1, X_2, X_3 \sim \mathcal{U}(-1, 1)$ be independently distributed and the true underlying relationship be defined by $Y = 3X_1\mathbb{1}_{X_3>0} - 3X_1\mathbb{1}_{X_3\leq 0} + X_3 + \epsilon$, with $\epsilon \sim \mathcal{N}(0, 0.09)$. We then draw 500 observations from these random variables and fit a feed-forward neural network (NN) with a single hidden layer of size 10 and weight decay of 0.001.⁹ The R^2 measured on a separately drawn test set of size 10000 following the same distribution is 0.94. The ICE and PD curves of feature \mathbf{x}_1 for the training data are shown in the left plot of Figure 2. The ICE curves clearly show that \mathbf{x}_1 influences the prediction differently depending on another feature—in this case, \mathbf{x}_3 . If we would only consider the global PD plot, the nearly-horizontal PD curve of \mathbf{x}_1 (grey line) would indicate no influence on the model’s predictions and thus is not representative for the underlying local feature effects (ICE curves). Here, REPID can be applied to the ICE curves of \mathbf{x}_1 to search for the best split point within the feature subset in $-j$ (here: \mathbf{x}_2 and \mathbf{x}_3) and minimize the feature interactions between features in j and $-j$. In this example, the best split point found is $\mathbf{x}_3 = 0$, which is also optimal according to the data-generating process. The regional PD plots found by REPID reflect the contradicting influence of feature \mathbf{x}_1 on the predictions compared to the global PD plot. The respective split reduces the interaction-related heterogeneity almost completely (by 98%). Hence, the resulting regional marginal effects of \mathbf{x}_1 can be approximated well by the respective main effects (regional PD), which are therefore more representative for the individual observations within each region.

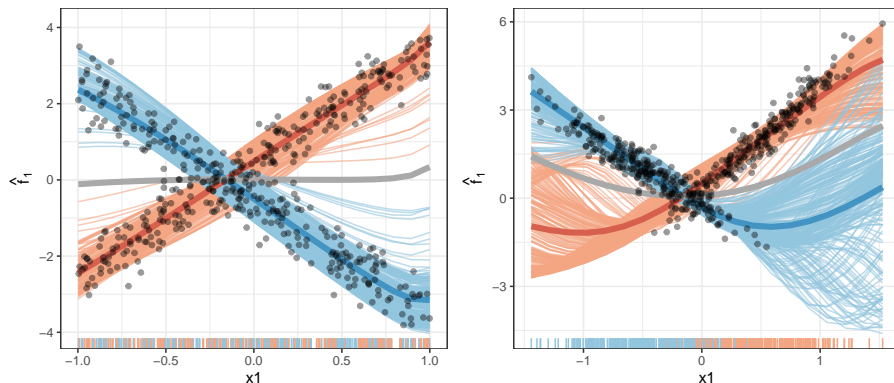


Figure 2: ICE curves and PD curves (grey) for the uncorrelated (left) and correlated case (right) of the simulation example of Section 3. ICE curves are colored w.r.t. the first split when REPID is applied. The split feature is in both cases \mathbf{x}_3 with split points -0.01 (left) and -0.15 (right). The blue color represents the left and orange the right region according to the split point. The thicker lines represent the respective regional PD curves. The rug plot shows the distribution of \mathbf{x}_1 according to the split point. The black points are the underlying observations.

9. The hyperparameters’ size (number of units of the hidden layer) and weight decay for a single-hidden-layer feed-forward NN were tuned via 5-fold cross-validation using grid search and a maximum of 1000 iterations. Considered grid values for weight decay: (0.5, 0.1, 0.01, 0.001, 0.0001, 0.00001), and for size: (3, 5, 10, 20, 30).

Herbinger et al. (2022) have shown that REPID provides meaningful results if 1) only one feature is of interest, and 2) if global feature effects are visualized by PD plots. These two assumptions limit the general applicability of REPID for two reasons.

First, applying REPID to different features of interest will usually result in different regions, as the method produces feature-specific regional PD plots. Hence, in the above-mentioned simulation example, REPID produces different regions when the feature of interest is \mathbf{x}_3 instead of \mathbf{x}_1 , which complicates interpretations when effects of multiple features are of interest. Moreover, we might be interested to receive regions within the feature space where interactions between multiple features are minimized, and thus the joint effect within each region can be decomposed into the main effects of the regarded features.

Second, there are other feature effect methods that might be more suitable, depending on the underlying data set and research question. Thus, a general framework that allows finding regions within the feature space where feature interactions are minimized w.r.t. an individually chosen feature effect method would be extremely useful. One main disadvantage specifically for ICE and PD plots is the extrapolation problem in the presence of feature interactions and correlations, as described in Section 2.3. To illustrate how this problem affects REPID, we consider the same simulation example as before, but with $X_1 = X_3 + \delta$ and $\delta \sim \mathcal{N}(0, 0.0625)$. We again draw 500 observations and fit an NN with the same specification and receive an R^2 of 0.92 on a separately drawn test set of size 10000 following the same distribution. Thus, the high correlation between \mathbf{x}_1 and \mathbf{x}_3 barely influences the model performance. However, Figure 2 clearly shows that ICE curves are extrapolating in low-density regions. The rug plot on the bottom indicates the distribution of feature \mathbf{x}_1 depending on feature \mathbf{x}_3 . Thus, the model was not trained on observations with small \mathbf{x}_1 values and simultaneously large \mathbf{x}_3 values, and vice versa. However, since we integrate over the marginal distribution, we also predict in these “out-of-distribution” areas. This leads to the so-called extrapolation problem and, hence, to uncertain predictions in extrapolated regions that must be interpreted with caution. In Section 6.1, we will analyze how severe the extrapolation problem is with regard to finding the correct split feature and split point.

4 Generalized Additive Decomposition of Global Effects (GADGET)

Here, we introduce a new framework called generalized additive decomposition of global effects (GADGET), which additively decomposes global feature effects based on minimizing feature interactions. Through this approach, one or multiple features (up to all p features) can be considered to find interpretable regions where feature effects of all regarded features are more representative for the underlying individual observations. We will first introduce the methodology of GADGET, which is applicable to many different feature effect methods. We formally define the axiom that must be satisfied by the desired feature effect method to be used in GADGET. We then show that the most popular feature effect methods satisfy this axiom and that REPID is a special case of GADGET.

4.1 The GADGET Algorithm

Let $h(x_j, \mathbf{x}_{-j}^{(i)})$ be the local feature effect of a feature \mathbf{x}_j of the i -th observation at some feature value $x_j \in \mathcal{X}_j$ measured by a local feature effect function $h : \mathbb{R}^p \rightarrow \mathbb{R}$, and let

$\mathbb{E}[h(x_j, X_{-j})|\mathcal{A}_g]$ be the expected feature effect of \mathbf{x}_j at x_j w.r.t. X_{-j} conditioned on the subspace $\mathcal{A}_g \subseteq \mathcal{X}$.¹⁰ Then, we can define the deviation between the local feature effect and the expected feature effect at a specific feature value x_j for subspace \mathcal{A}_g using a point-wise loss function, e.g., the squared distance¹¹:

$$\mathcal{L}(\mathcal{A}_g, x_j) = \sum_{i:\mathbf{x}^{(i)} \in \mathcal{A}_g} \left(h(x_j, \mathbf{x}_{-j}^{(i)}) - \mathbb{E}[h(x_j, X_{-j})|\mathcal{A}_g] \right)^2. \quad (10)$$

The risk function \mathcal{R} of the j -th feature and subspace \mathcal{A}_g is defined by aggregating the point-wise loss of Eq. (10) over a sample of feature values of \mathbf{x}_j :

$$\mathcal{R}(\mathcal{A}_g, \mathbf{x}_j) = \sum_{k:k \in \{1, \dots, m\} \wedge \mathbf{x}_j^{(k)} \in \mathcal{A}_g} \mathcal{L}(\mathcal{A}_g, \mathbf{x}_j^{(k)}). \quad (11)$$

For instance, feature values of size m can be sampled values of \mathbf{x}_j .¹² and their constraint depends on feasible values within the subspace \mathcal{A}_g .

The local feature effect function must be defined in such a way that the risk function in Eq. (11) minimizes the interaction-related heterogeneity of features in S , i.e., the feature interactions between $\mathbf{x}_j \in \mathbf{x}_S$ with $S \subseteq \{1, \dots, p\}$ and features of a previously defined feature set $Z \subseteq \{1, \dots, p\}$ (see Section 4.2). The feature subset S is chosen to be the subset of features for which we want to receive representative regional feature effect plots by minimizing their interaction-related heterogeneity. Features in Z are considered as split features and thus aim to partition the feature space in such a way that feature interactions with features in S are minimized. Algorithm 1 defines a single partitioning step of GADGET, which is inspired by the CART algorithm (Breiman et al., 1984) and is recursively repeated until a certain stop criterion is met (see Section 4.7). We greedily search for the best split point within the feature subset Z such that the interaction-related heterogeneity of feature subset S is minimized in the two resulting subspaces. The interaction-related heterogeneity is measured by the variance of the local feature effects of \mathbf{x}_j within the new subspace (see Eq. 11). Hence, for each split feature z and split point t , we sum up the risk of the two resulting subspaces for all features in S (line 6 in Algorithm 1) and then choose the split point of the split feature (\hat{t}, \hat{z}) that minimizes the interaction-related heterogeneity of all features $j \in S$ (line 9 in Algorithm 1).¹³

4.2 Theoretical Foundation of GADGET

To apply GADGET, a suitable local feature effect function h must be defined. General properties that GADGET requires from this function are provided by Axiom 1.

-
10. The expected value is always taken w.r.t. the random variables within the expected value. We only use a subscript for the expected value if it cannot uniquely be defined by the above notation.
 11. Other distance metrics are also possible. However, we chose the squared distance, since the interpretation in terms of variance is most intuitive in this context.
 12. The choice depends on the underlying local feature effect function h and on the data distribution. Other common choices are quantiles, or an equidistant grid from the feature range of \mathbf{x}_j .
 13. In the case where $z \in S$, we also include the heterogeneity reduction of the z -th feature in the objective, since we aim to reduce the overall interaction-related heterogeneity of all features in S .
 14. S and Z can be distinct or partially or fully overlap with each other. See Section 5 for defining S and Z .

Algorithm 1: Partitioning algorithm of GADGET

- 1: **input:** subspace $\mathcal{A} \subseteq \mathcal{X}$, risk function \mathcal{R} and feature of interest index set $S \subseteq \{1, \dots, p\}$ and feature interaction index set $Z \subseteq \{1, \dots, p\}$ ¹⁴
 - 2: **output:** subspaces $\mathcal{A}_l^{\hat{t}, \hat{z}}$ and $\mathcal{A}_r^{\hat{t}, \hat{z}}$
 - 3: **for** each feature indexed by $z \in Z$ **do**
 - 4: **for** every split t on feature \mathbf{x}_z **do**
 - 5: $\mathcal{A}_l^{t,z} = \{\mathcal{A} | \mathbf{x}_z \leq t\}$; $\mathcal{A}_r^{t,z} = \{\mathcal{A} | \mathbf{x}_z > t\}$
 - 6: $\mathcal{I}(t, z) = \sum_{j \in S} \left(\mathcal{R}(\mathcal{A}_l^{t,z}, \mathbf{x}_j) + \mathcal{R}(\mathcal{A}_r^{t,z}, \mathbf{x}_j) \right)$
 - 7: **end for**
 - 8: **end for**
 - 9: Choose $(\hat{t}, \hat{z}) \in \arg \min_{t,z} \mathcal{I}(t, z)$
-

Axiom 1 (Local Decomposability) A local feature effect function $h : \mathbb{R}^p \rightarrow \mathbb{R}$ satisfies the local decomposability axiom if and only if the decomposition of the i -th local effect $h(x_j, \mathbf{x}_{-j}^{(i)})$ of feature \mathbf{x}_j at x_j solely depends on main and higher-order effects of feature \mathbf{x}_j :

$$h(x_j, \mathbf{x}_{-j}^{(i)}) = g_j(x_j) + \sum_{k=1}^{p-1} \sum_{\substack{W \subseteq -j, \\ |W|=k}} g_{W \cup j}(x_j, \mathbf{x}_W^{(i)}).$$

The *local decomposability* axiom must be satisfied by the chosen local feature effect function h . Thus, the i -th local feature effect $h(x_j, \mathbf{x}_{-j}^{(i)})$ for feature \mathbf{x}_j at x_j must be defined such that it only depends on the main effect of feature \mathbf{x}_j as well as the interaction effects between \mathbf{x}_j and all other features in $-j$. This decomposition is not generally given by every local feature effect method. For example, the decomposition of ICE curves depends not only on effects including the feature of interest \mathbf{x}_j but also on effects of other features, which leads to additive shifts. However, we can usually transform the local feature effects in a meaningful manner to receive the decomposition provided in Axiom 1. ICE curves, for instance, must be mean-centered (see Appendix B.4) to satisfy the *local decomposability* axiom. If the local feature effect function satisfies Axiom 1, then Theorem 2 guarantees that the loss function defined in Eq. (10) quantifies the interaction-related heterogeneity of local effects (feature interactions) of feature \mathbf{x}_j at x_j within the regarded subspace \mathcal{A}_g .

Theorem 2 If the local feature effect function $h(x_j, \mathbf{x}_{-j}^{(i)})$ satisfies Axiom 1, then the loss function $\mathcal{L}(\mathcal{A}_g, x_j)$ defined in Eq. (10) only depends on feature interactions between the feature \mathbf{x}_j at x_j and features in $-j$:

$$\mathcal{L}(\mathcal{A}_g, x_j) = \sum_{i: \mathbf{x}^{(i)} \in \mathcal{A}_g} \left(\sum_{k=1}^{p-1} \sum_{\substack{W \subseteq -j, \\ |W|=k}} g_{W \cup j}(x_j, \mathbf{x}_W^{(i)}) - \mathbb{E}[g_{W \cup j}(x_j, X_W) | \mathcal{A}_g] \right)^2.$$

The proof can be found in Appendix B.1.

Since we only use features in Z for splitting and we aggregate the resulting risk over all features $j \in S$, the objective function in GADGET minimizes the feature interactions between all features in S and interacting features in Z (see Theorem 3). Furthermore, if Z contains all features interacting with any feature in S (i.e., no feature in $-Z$ interacts with any feature in S), then the theoretical minimum of the objective minimized in Algorithm 1 is zero (see Corollary 4). This means that all feature interactions present in feature effects of the features in S can be reduced such that only main effects of these features remain in each subspace. Thus, the joint feature effect $f_{S|\mathcal{A}_g}$ within each subspace \mathcal{A}_g can be uniquely and additively decomposed into the univariate feature effects $f_{j|\mathcal{A}_g}$:

$$f_{S|\mathcal{A}_g}(\mathbf{x}_S) = \sum_{j \in S} f_{j|\mathcal{A}_g}(\mathbf{x}_j). \quad (12)$$

However, if Z is chosen such that the features contained in its complement $-Z$ interact with features contained in S , then the theoretical minimum of the objective is larger than 0. Thus, heterogeneous effects due to feature interactions between features in S and features in $-Z$ remain. The approach to choose the subsets S and Z is discussed in Section 5.

Theorem 3 *If the local feature effect function h satisfies Axiom 1 and if all features contained in Z and all features in $-Z = Z^c$ are pairwise independent, then the objective function $\mathcal{I}(t, z)$ of Algorithm 1 based on the loss function in Eq. (10) minimizes feature interactions between features within the subset S and features in Z , but does not generally minimize feature interactions between features in S and $-Z$. Since the partitions found by the GADGET algorithm to minimize the feature interactions of S only depend on features in Z and are independent of features in $-Z$, interactions between each $j \in S$ and features in $-Z$ are independent of the partitioning in Algorithm 1:*

$$\left(\sum_{l=1}^{|-Z \setminus j|} \sum_{\substack{-Z_l \subseteq -Z \setminus j, \\ |-Z_l|=l}} g_{-Z_l \cup j}(x_j, \mathbf{x}_{-Z_l}^{(i)}) - \mathbb{E}[g_{-Z_l \cup j}(x_j, X_{-Z_l}) | \mathcal{A}_b^{t,z}] \right) \perp\!\!\!\perp \mathcal{A}_b^{t,z}.$$

The proof can be found in Appendix B.2.

Corollary 4 *If the local feature effect function h satisfies Axiom 1 and if the feature subset $-Z = Z^c$ does not contain any features interacting with any $j \in S$, then the theoretical minimum of the objective function in Algorithm 1 is $\mathcal{I}(t^*, z^*) = 0$.*

The proof can be found in Appendix B.3.

The fulfillment of the *local decomposability* axiom depends on the definition of the underlying local feature effect function h . In the following sections, we show the validity of this axiom for common feature effect methods and provide estimates as well as visualizations for the resulting regional effect curves and their remaining interaction-related heterogeneity.

4.3 GADGET-PD

Here, we show the applicability of PD as feature effect method within the GADGET algorithm which we call the GADGET-PD.

Method. The PD plot is based on ICE curves (local feature effects) and one of the most popular global feature effect methods. However, ICE curves of feature \mathbf{x}_j do not satisfy Axiom 1, since the decomposition of the i -th ICE curve also contains main or interaction effects of the i -th observation that are independent of feature \mathbf{x}_j (see Appendix B.4). These effects can be cancelled out by centering ICE curves w.r.t. the mean of each curve (i.e., $\mathbb{E}[\hat{f}(X_j, \mathbf{x}_{-j}^{(i)})]$). The resulting mean-centered ICE curves satisfy Axiom 1 (see Appendix B.4). Hence, they are chosen as local feature effect method within GADGET: $h(x_j, \mathbf{x}_{-j}^{(i)}) = \hat{f}^c(x_j, \mathbf{x}_{-j}^{(i)}) = \hat{f}(x_j, \mathbf{x}_{-j}^{(i)}) - \mathbb{E}[\hat{f}(X_j, \mathbf{x}_{-j}^{(i)})|\mathcal{A}_g]$.

The loss function used within GADGET-PD to minimize the interaction-related heterogeneity is then defined by the variability of mean-centered ICE curves:

$$\mathcal{L}^{PD}(\mathcal{A}_g, x_j) = \sum_{i: \mathbf{x}^{(i)} \in \mathcal{A}_g} \left(\hat{f}^c(x_j, \mathbf{x}_{-j}^{(i)}) - \mathbb{E}[\hat{f}^c(x_j, X_{-j})|\mathcal{A}_g] \right)^2. \quad (13)$$

By choosing mean-centered ICE curves as local feature effect function h , the loss function in Eq. (13) for GADGET-PD results in the same loss function used within REPID. In Appendix B.4, we show that the REPID method is—for this specific loss function—a special case of GADGET-PD, where we have only one feature of interest (i.e., $S = j$) and where we consider all other features to be potential split features (i.e., $Z = -j$).

Note that since REPID never splits with regard to the visualized feature of interest \mathbf{x}_j , the constant used for mean-centering (i.e., $\mathbb{E}[\hat{f}(X_j, \mathbf{x}_{-j}^{(i)})|\mathcal{A}_g] = \mathbb{E}[\hat{f}(X_j, \mathbf{x}_{-j}^{(i)})]$) always stays the same. In contrast, for the more general GADGET algorithm, the mean-centering constant depends on how S and Z are defined. Thus, the mean-centering constants of features in S might change if we also use them for splitting. For example, in Figure 3, we use feature \mathbf{x}_3 as a feature of interest in S and as a split feature in Z . In this case, the range of the visualized feature \mathbf{x}_3 is also split according to the split point found by the GADGET algorithm. Hence, the expected value conditioned on the new subspace changed (i.e., $\mathbb{E}[\hat{f}(X_j, \mathbf{x}_{-j}^{(i)})|\mathcal{A}_g] \neq \mathbb{E}[\hat{f}(X_j, \mathbf{x}_{-j}^{(i)})]$) and thus must be adjusted to avoid additive (non-interaction) effects in the new subspace.

Illustration. Figure 3 visualizes the result when applying GADGET-PD on the uncorrelated simulation example of Section 3 by choosing $S = Z = \{1, 2, 3\}$. Hence, we are interested in the feature effect of all available features and consider all features as possible interaction (split) features. GADGET-PD performs one split with regard to $\mathbf{x}_3 \approx 0$. Thus, the correct split feature and its corresponding split point are found by GADGET such that the interaction-related heterogeneity of all features in S is almost completely reduced and only main effects within the subspaces remain.

Decomposition. If Z contains all features interacting with features in S and if GADGET is applied such that the theoretical minimum of the objective function is reached, then according to Corollary 4, the joint mean-centered PD function $f_{S|\mathcal{A}_g}^{PD,c}$ within each final subspace \mathcal{A}_g can be decomposed into the respective 1-dimensional mean-centered PD functions:

$$f_{S|\mathcal{A}_g}^{PD,c}(\mathbf{x}_S) = \sum_{j \in S} f_{j|\mathcal{A}_g}^{PD,c}(\mathbf{x}_j). \quad (14)$$

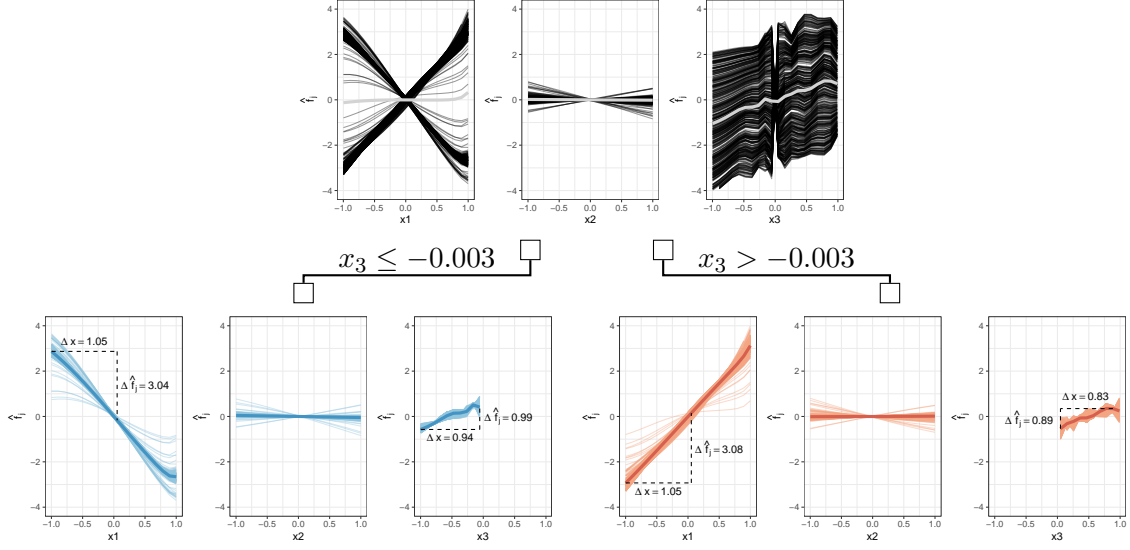


Figure 3: Visualization of applying GADGET with $S = Z = \{1, 2, 3\}$ to mean-centered ICE curves of the uncorrelated simulation example of Section 3 with $Y = 3X_1 \mathbb{1}_{X_3 > 0} - 3X_1 \mathbb{1}_{X_3 \leq 0} + X_3 + \epsilon$ with $\epsilon \sim \mathcal{N}(0, 0.09)$. The upper plots show the mean-centered ICE and PD curves on the entire feature space, while the lower plots represent the respective mean-centered ICE and PD curves after partitioning the feature space w.r.t. $\mathbf{x}_3 = -0.003$.

Eq. (14) is justified by the assumption that no more interactions between features in S and other features are present in the final regions (Friedman and Popescu, 2008).

Furthermore, if the subset $-S$ is the subset of features that do not interact with any other features (local feature effects are homogeneous), then according to Eq. (14) and Eq. (4), the prediction function $\hat{f}_{\mathcal{A}_g}$ within each final subspace \mathcal{A}_g can be decomposed into the 1-dimensional mean-centered PD functions of all p features plus a constant value g_0 :

$$\hat{f}_{\mathcal{A}_g}(\mathbf{x}) = g_0 + \sum_{j=1}^p f_{j|\mathcal{A}_g}^{PD,c}(\mathbf{x}_j).$$

Thus, depending on how we choose the subsets S and Z and the extent to which we are able to minimize the interaction-related heterogeneity of feature effects by recursively applying Algorithm 1, we might be able to approximate the prediction function by an additive function of main effects of all features within the final regions.

This can also be shown for the simulation example illustrated in Figure 3, where $\hat{f}_{2|\mathcal{A}_g}^{PD,c}(\mathbf{x}_2) = 0$ (the regional effect of feature \mathbf{x}_2 after the split is still 0 and has low interaction-related heterogeneity). Instead, the regional effects of \mathbf{x}_1 and \mathbf{x}_3 vary compared to the root node and strongly reduce the interaction-related heterogeneity. Since the regional effects of \mathbf{x}_1 and \mathbf{x}_3 are approximately linear, we can estimate the prediction function

within each subspace by

$$\hat{f}_{\mathcal{A}_l}(\mathbf{x}) = g_0 + \frac{-3.04}{1.05}\mathbf{x}_1 + \frac{0.99}{0.94}\mathbf{x}_3 = g_0 - 2.9\mathbf{x}_1 + 1.05\mathbf{x}_3$$

and

$$\hat{f}_{\mathcal{A}_r}(\mathbf{x}) = g_0 + \frac{3.08}{1.05}\mathbf{x}_1 + \frac{0.89}{0.83}\mathbf{x}_3 = g_0 + 2.93\mathbf{x}_1 + 1.07\mathbf{x}_3,$$

which is a close approximation to the underlying data-generating process and thus provides a better understanding of how the features of interest influence the prediction function compared to only considering the global PD plots.

Note that besides the decomposability property in Eq. (14), each global PD of features in S is a weighted additive combination of the final regional PDs. Thus, each global PD can be additively decomposed into regional PD.

Estimates and Visualization. To estimate and visualize the expected regional effect, one can choose between the regional PD curve $\hat{f}_{j|\mathcal{A}_g}^{PD}$ or its mean-centered version $\hat{f}_{j|\mathcal{A}_g}^{PD,c}$ for each feature $j \in S$, which are calculated by Monte-Carlo integration for each final region \mathcal{A}_g . The interaction-related heterogeneity for each feature in S and final subspace \mathcal{A}_g is measured by the risk function in Eq. (11) with the loss function in Eq. (13). Thus, the interaction-related heterogeneity quantifies the variation of mean-centered ICE curves within each region. For visualization purposes, we calculate the 95% intervals of interaction-related heterogeneity based on this variation. We then suggest a plot for each feature in S that shows the final regional PD curves and 95% interaction-related heterogeneity intervals (see e.g., Figure 11).

The main issue with local ICE curves and resulting global PD plots is the extrapolation problem when features are correlated, as demonstrated in Section 3. This problem remains for GADGET when mean-centered ICE curves are chosen as local feature effect function h .

4.4 GADGET-ALE

An alternative global feature effect method that allows an additive decomposition of the prediction function and the interpretation of individual feature effects are ALE plots (Apley and Zhu, 2020), which we summarized in Section 2.3. Here, we show their applicability within the GADGET algorithm which we term GADGET-ALE.

Method. While ALE curves compared to PD curves do not suffer from extrapolation, they do not directly entail a local feature effect visualization that shows the heterogeneity induced by feature interactions as ICE curves for PD plots. However, ALE plots are also based on corresponding local feature effects that provide information about the underlying interaction-related heterogeneity and that can be used within the GADGET algorithm to receive more representative ALE curves in the final regions. These local feature effects are the derivatives w.r.t. the feature of interest \mathbf{x}_j of the prediction function (see Eq. 5). In Appendix B.5, we show that by choosing $h = \frac{\partial \hat{f}(x_j, \mathbf{x}_{-j}^{(i)})}{\partial x_j}$, Axiom 1 is met, which leads to the following loss function used within the objective in GADGET-ALE:

$$\mathcal{L}^{ALE}(\mathcal{A}_g, x_j) = \sum_{\substack{i: \mathbf{x}^{(i)} \in \mathcal{A}_g \wedge \\ \mathbf{x}^{(i)} \in \mathbb{P}(\mathbf{x}_{-j}|x_j)}} \left(\frac{\partial \hat{f}(x_j, \mathbf{x}_{-j}^{(i)})}{\partial x_j} - \mathbb{E} \left[\frac{\partial \hat{f}(X_j, X_{-j})}{\partial x_j} \middle| \mathcal{A}_g \wedge X_j = x_j \right] \right)^2. \quad (15)$$

The derivatives are calculated by defining m intervals for feature \mathbf{x}_j and quantifying for each interval the prediction difference between the upper and lower boundary for observations lying in this interval (see Eq. 6). Hence, the loss function in Eq. (15) measures the variance of the derivatives of observations where the feature values of \mathbf{x}_j lie within the boundaries of the regarded interval and, thus, measures the interaction-related heterogeneity of local effects of feature \mathbf{x}_j within this interval. The risk function in Eq. (11) then aggregates this loss over all m intervals. Note that the conditional expectation in Eq. (15) is the expected conditional derivative (estimated by the average derivative within the regarded interval) and not the ALE curve itself. However, the ALE curve is calculated by integrating the expected conditional derivative up to the regarded value x_j (see Eq. 5).

Illustration. Figure 4 illustrates the first split for the two simulation examples of Section 3 using GADGET-ALE. The heterogeneity of the local effects (derivatives) before applying GADGET is very high, spanning across negative to positive values (grey boxplots) within each interval. With GADGET, we then partition the feature space w.r.t. one of the features in Z such that this interaction-related heterogeneity is minimized. When GADGET-ALE is used, for both the uncorrelated and the correlated case, we receive the correct split feature and approximately the correct split point, which clearly shows a high reduction in heterogeneity of these local effects after the first split. While the shapes of the centered ALE curves look very similar to PD plots (see Figure 2) for the uncorrelated case, the ALE curves for the correlated case do not extrapolate and, thus, are more representative for the feature effect with regard to the underlying data distribution.

Decomposition Equivalently to PD plots, ALE plots also contain an additive recovery and, thus, can be decomposed additively into main and interaction effects (see Section 2.3). Furthermore, if Z is defined such that all features interacting with features in S are included and if GADGET is applied so that the theoretical minimum of the objective function is reached, then—according to Corollary 4—the joint mean-centered ALE function $f_{S|\mathcal{A}_g}^{ALE,c}$ within each final subspace \mathcal{A}_g can be decomposed into the 1-dimensional mean-centered ALE functions of features in S (see Eq. 12). Thus, for ALE plots, we might also be able to decompose the prediction function into the regional features’ main effects, depending on how we choose the subsets S and Z within the GADGET algorithm. More details on the decomposition when using GADGET-ALE and an exemplary illustration of the uncorrelated simulation example of Section 3 can be found in Appendix C.1.

Estimates and Visualization. The regional effect is estimated by the regional centered ALE curve $\hat{f}_{j|\mathcal{A}_g}^{ALE,c}$ for each feature in S and is calculated as in Eq. (6) for each final subspace \mathcal{A}_g . The interaction-related heterogeneity for each feature in S and final subspace \mathcal{A}_g is measured by the risk function in Eq. (11) with the loss function in Eq. (15). Thus, the interaction-related heterogeneity quantifies the variation of partial derivatives within each subspace. Since the partial derivatives cannot be meaningfully visualized within the ALE plot itself, we suggest to visualize it in combination with a plot for the interaction-related heterogeneity measured by the standard deviation of partial derivatives within each interval, which is inspired by the derivative ICE plots of Goldstein et al. (2015) (see e.g., Figure 12).

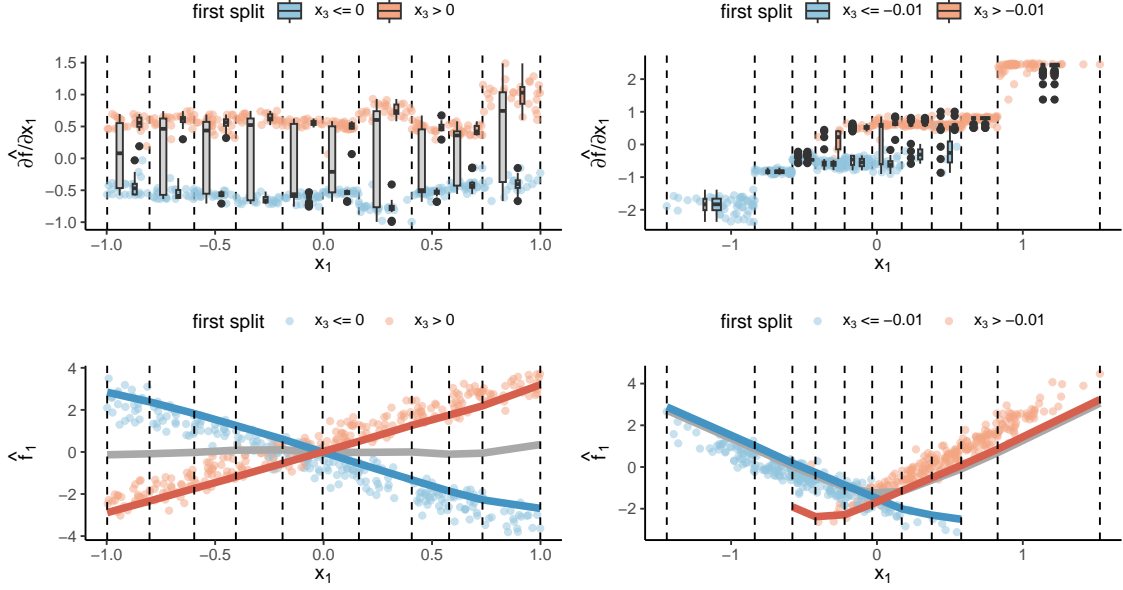


Figure 4: Visualization of derivatives of \hat{f} w.r.t. \mathbf{x}_1 (top) and respective ALE curves (bottom) for the uncorrelated (left) and correlated case (right) of the simulation example of Section 3, with $Y = 3X_1 \mathbb{1}_{X_3 > 0} - 3X_1 \mathbb{1}_{X_3 \leq 0} + X_3 + \epsilon$ and $\epsilon \sim \mathbb{N}(0, 0.09)$. Derivatives (top) and mean-centered observational values (bottom) are colored w.r.t. the first split when GADGET-ALE with $S = 1$ and $Z = \{2, 3\}$ is applied. The boxplots (top) and lines (bottom) in grey show the variation of derivatives and the global centered ALE curves, respectively. The colored curves show the regional centered ALE curves after the first split with GADGET-ALE.

4.5 GADGET-SD

While PD and ALE plots visualize the global feature effect for which we define the appropriate local feature effect function (mean-centered ICE curves and derivatives) for the GADGET algorithm, the SD plot (Section 2.3) is comparable to an ICE plot and, thus, does not show the global feature effect itself. Here, we provide an estimate for the global effect and show the applicability of SD within GADGET which we term GADGET-SD.

Method. Herren and Hahn (2022) (amongst others) showed that the Shapley value $\phi_j^{(i)}(x_j)$ of observation i for feature value $x_j = \mathbf{x}_j^{(i)}$ can be decomposed as defined in Eq. (8) to

$$\phi_j^{(i)}(x_j) = g_j^c(x_j) + \sum_{k=1}^{p-1} \frac{1}{k+1} \sum_{W \subseteq -j: |W|=k} g_{W \cup j}^c(x_j, \mathbf{x}_W^{(i)}),$$

with $g_{W \cup j}^c(x_j, \mathbf{x}_W^{(i)}) = \mathbb{E}[\hat{f}(x_j, X_{-j}) | X_W = \mathbf{x}_W^{(i)}] - \sum_{V \subset \{W \cup j\}} \mathbb{E}[\hat{f}(X) | X_V = \mathbf{x}_V^{(i)}]$, which satisfies Axiom 1 (see Appendix B.6). The global feature effect for the SD plot of feature

\mathbf{x}_j at the feature value $x_j = \mathbf{x}_j^{(i)}$ can then be defined by

$$f_j^{SD}(x_j) = \mathbb{E}_{X_W}[\phi_j(x_j)] = g_j^c(x_j) + \sum_{k=1}^{p-1} \frac{1}{k+1} \sum_{W \subseteq -j: |W|=k} \mathbb{E}[g_{W \cup j}^c(x_j, X_W)]. \quad (16)$$

Following from that, according to Theorem 2, the respective loss function used in GADGET depends only on interaction effects between \mathbf{x}_j and features in $-j$ and is given by

$$\mathcal{L}^{SD}(\mathcal{A}_g, x_j) = \sum_{i: \mathbf{x}^{(i)} \in \mathcal{A}_g \wedge \mathbf{x}_j^{(i)} = x_j} \left(\phi_j^{(i)}(x_j) - \mathbb{E}_{X_W}[\phi_j(x_j) | \mathcal{A}_g] \right)^2. \quad (17)$$

For more details, see Appendix B.

While there exist estimators for the global effect in PD and ALE plots, a pendant for the SD plot has not been introduced yet. Hence, a suitable estimator to estimate the expected value of Shapley values of feature \mathbf{x}_j in Eq. (17) must be chosen. Here, we use univariate GAMs with splines to estimate the expected value.¹⁵ Thus, the estimated GAM for feature \mathbf{x}_j represents the regional SD feature effect of feature \mathbf{x}_j within subspace \mathcal{A}_g .

Illustration. Figure 5 visualizes the SD plot for feature \mathbf{x}_1 of the simulation example described in Section 3. Similarly to the least-square estimate in linear regression, we search for the GAM that minimizes the squared distance (Δ^2) of the Shapley values of \mathbf{x}_1 . With GADGET, we now split such that the fitted GAMs within the two new subspaces minimize the squared distances between them and the Shapley values within the respective subspace. Since the GAMs are fitted on the Shapley values (local feature effects), in contrast to PDs, they do not extrapolate with regard to \mathbf{x}_1 in the correlated scenario. However, as defined in the beginning of this section, Shapley values are based on expected values that must be estimated. If they are calculated using the interventional approach (as we do here), it is still possible that the predictions considered in the Shapley values extrapolate in sparse regions. Hence, the definition of Shapley values via expected values differs from those of ICE curves and derivatives for ALE, which are based on local predictions. Similarly to estimating the mean-centering constants for ICE curves, it follows that the expected values within the Shapley value estimation must consider the regarded subspace \mathcal{A}_g to acknowledge the full heterogeneity reduction due to interactions within each subspace. This means that we must recalculate the Shapley values after each partitioning step for each new subspace to receive regional SD effects in the final subspaces that are representative of the underlying main effects within each subspace. However, without recalculating the conditional expected values, we still minimize the unconditional expected value (i.e., the feature interactions on the entire feature space). The two different approaches lead to a different acknowledgment of interaction effects. In general, it can be said that the faster approach without recalculation will be less likely to detect feature interactions of higher order compared to the exact approach with recalculation. The differences of the two approaches for the simulation example of Section 3 are explained in Appendix C.2 and further discussed on a more complex simulation example in Section 6.2.

15. Splines are functions that are defined in a piece-wise manner by polynomials. Splines are often preferred over polynomial regression, since they provide more flexibility with already low-order polynomials.

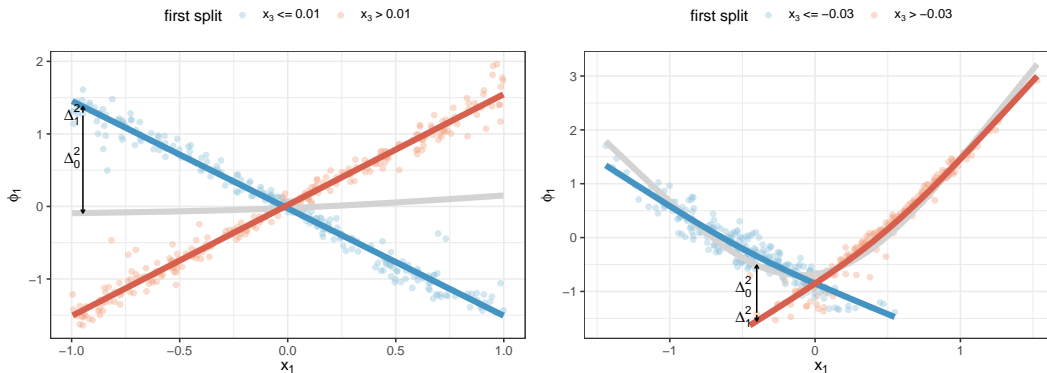


Figure 5: Visualization of Shapley values ϕ_1 w.r.t. \mathbf{x}_1 for the uncorrelated (left) and correlated case (right) of the simulation example of Section 3, with $Y = 3X_1 \mathbb{1}_{X_3 > 0} - 3X_1 \mathbb{1}_{X_3 \leq 0} + X_3 + \epsilon$ and $\epsilon \sim \mathcal{N}(0, 0.09)$. Shapley values (points) and the respective regional feature effect curves (GAMs) are colored w.r.t. the first split when GADGET-SD with $S = 1$ and $Z = \{2, 3\}$ is applied. The grey curve represents the global feature effect based on the entire feature space. Δ_0^2 represents the squared distance between a given Shapley value and the global SD curve (grey), while Δ_1^2 measures the squared distance between this Shapley value and the respective regional SD curve. The GAMs are fitted such that these squared distances over all Shapley values in the respective regions are minimized.

Decomposition. The decomposition of Shapley values differs from that of mean-centered ICE curves in the way that feature interactions in Shapley values are fairly distributed between involved features, which leads to decreasing weights the higher the order of the interaction effect (see Eq. 8). In contrast, all interaction terms receive the same weight as the main effects in ICE curves. Hence, interactions of high order lead to less heterogeneity in SD plots compared to ICE plots. However, by using the interventional approach to calculate Shapley values, they can be decomposed by weighted PD functions (see Eq. 8 and Herren and Hahn, 2022). Hence, the same decomposition rules as defined for PD plots apply for the SD feature effect, as defined in Eq. (16). Meaning, if Z contains all features interacting with features in S , and if GADGET is applied such that the theoretical minimum of the objective function is reached, then according to Corollary 4, the regional joint SD effect of features in S can be decomposed into 1-dimensional regional SD effect functions, as in Eq. (12). In this special case and if Shapley values are estimated by the interventional approach, it can be shown that $f_{j|\mathcal{A}_g}^{SD,c} = f_{j|\mathcal{A}_g}^{PD,c}$ (see Appendix C.2).

Again, we might be able to decompose the prediction function into the regional features' main effects, depending on how we choose the feature subsets S and Z within the GADGET algorithm. More details and an exemplary illustration of the uncorrelated simulation example of Section 3 can be found in Appendix C.2.

Estimates and Visualization. The regional SD effect is estimated by a GAM for each feature in S and final region \mathcal{A}_g . The interaction-related heterogeneity for each feature in

S and final subspace \mathcal{A}_g is measured by the risk function in Eq. (11) with the loss function in Eq. (17). The risk function quantifies the variation of Shapley values of feature \mathbf{x}_j within each region. We visualize the interaction-related heterogeneity by the Shapley values that are recalculated conditioned on the subspace \mathcal{A}_g (see, e.g., Figure 18 in Appendix E).

An overview of introduced estimates and visualization techniques for the different effect methods can be found in Appendix C.3. Moreover, an explanation of how categorical features are handled within GADGET for each of the presented feature effect methods is provided in Appendix C.4.

4.6 Quantifying Feature Interactions

Since GADGET minimizes the interaction-related heterogeneity based on the underlying feature effect method, we can quantify feature interactions by measuring the heterogeneity reduction in each partitioning step. We introduce several measures (inspired by Herbringer et al., 2022) to gain more insights into learned feature interactions and the meaningfulness of the final regional effects based on the interaction-related heterogeneity reduction.

Analysis of Single Partitioning Steps. We can quantify the extent to which interaction-related heterogeneity has been reduced in each of the features in S after splitting according to the chosen split feature $z \in Z$. Here, we denote G to be the total number of nodes after applying GADGET. Furthermore, we denote P to be the index of a parent node and the indices l and r to be the respective child nodes. We can quantify the relative interaction-related heterogeneity reduction after the respective partitioning step for feature $j \in S$ by

$$I(\mathcal{A}_P, \mathbf{x}_j) = \frac{\mathcal{R}(\mathcal{A}_P, \mathbf{x}_j) - \mathcal{R}(\mathcal{A}_l, \mathbf{x}_j) - \mathcal{R}(\mathcal{A}_r, \mathbf{x}_j)}{\mathcal{R}(\mathcal{X}, \mathbf{x}_j)},$$

meaning that we quantify the risk reduction of the regarded split relative to the risk on the entire feature space (root node) for one feature of interest $j \in S$. For example, in Figure 3, the interaction-related heterogeneity reduction of the first split ($I(\mathcal{X}, \mathbf{x}_1)$) for feature \mathbf{x}_1 is 0.986, which means that almost all of the interaction-related heterogeneity of \mathbf{x}_1 is reduced after the first split.

Analysis of Single Split Features. Instead of considering only a single partitioning step, one might be more interested in how much interaction-related heterogeneity reduction a specific split feature $z \in Z$ is responsible for w.r.t. all performed partitioning steps of an entire tree. To that end, we can quantify (either for each feature of interest in S or for all features in S together) the relative amount of heterogeneity reduction due to feature z . Hence, we receive $I_{z,j}(\mathbf{x}_j)$ by summing up $I(\mathcal{A}_P, \mathbf{x}_j)$ for the set of parent subspaces that used feature z as split feature and that we denote by $\mathcal{B}_z \subset \{\mathcal{A}_1, \dots, \mathcal{A}_G\}$:

$$I_{z,j}(\mathbf{x}_j) = \sum_{\mathcal{A}_P \in \mathcal{B}_z} I(\mathcal{A}_P, \mathbf{x}_j).$$

We obtain the overall interaction-related heterogeneity reduction I_z of the z -th split feature by first aggregating over all features in S :

$$I_z = \frac{\sum_{\mathcal{A}_P \in \mathcal{B}_z} \sum_{j \in S} (\mathcal{R}(\mathcal{A}_P, \mathbf{x}_j) - \mathcal{R}(\mathcal{A}_l, \mathbf{x}_j) - \mathcal{R}(\mathcal{A}_r, \mathbf{x}_j))}{\sum_{j \in S} \mathcal{R}(\mathcal{X}, \mathbf{x}_j)}.$$

In our previous example, we obtain $I_{3,1}(\mathbf{x}_1) = I(\mathcal{X}, \mathbf{x}_1) = 0.986$, since $z = 3$ was only used once for splitting, while the interaction-related heterogeneity reduction of all three features is $I_3 = 0.99$ for $z = 3$.

Goodness of Fit. A further aggregation level would be to sum up $I_{z,j}(\mathbf{x}_j)$ over all $z \in Z$ and, thus, receive the interaction-related heterogeneity reduction for feature \mathbf{x}_j between the entire feature space and the final subspaces (hence, over the entire tree). This is related to the concept of R^2 , which is a well-known measure in statistics to quantify the goodness of fit. We apply this concept here to quantify how well the final regional effect curves (in the final subspaces $\mathcal{B}_t \subset \{\mathcal{A}_1, \dots, \mathcal{A}_G\}$) fit the underlying local effects compared to the global feature effect curve on the entire feature space. We distinguish between the feature-related R_j^2 , which represents the goodness of fit for the feature effects of feature \mathbf{x}_j :

$$R_j^2 = \sum_{z \in Z} I_{z,j}(\mathbf{x}_j) = 1 - \frac{\sum_{\mathcal{A}_t \in \mathcal{B}_t} \mathcal{R}(\mathcal{A}_t, \mathbf{x}_j)}{\mathcal{R}(\mathcal{X}, \mathbf{x}_j)},$$

and the R_{Tot}^2 , which quantifies the goodness of fit for the feature effects of all features in S :

$$R_{Tot}^2 = \sum_{z \in Z} I_z = 1 - \frac{\sum_{\mathcal{A}_t \in \mathcal{B}_t} \sum_{j \in S} \mathcal{R}(\mathcal{A}_t, \mathbf{x}_j)}{\sum_{j \in S} \mathcal{R}(\mathcal{X}, \mathbf{x}_j)}.$$

Both R^2 measures take values between 0 and 1, with values close to 1 signalling that almost all heterogeneity in the final subspaces compared to the entire feature space has been reduced—either for a specific feature of interest (R_j^2) or for all features of interest (R_{Tot}^2). In our example, R_1^2 for feature \mathbf{x}_1 is the same as for $I_{3,1}(\mathbf{x}_1)$, since GADGET performed only one split. The total interaction-related heterogeneity reduction over all features in S is $R_{Tot}^2 = I_3 = 0.99$. Hence, the interaction-related heterogeneity of all features in S has been reduced by 99% after the first split.

These measures provide a tool set to better understand how features interact with each other and how well the final regional effect plots represent the underlying local effects.

4.7 Choosing Stop Criteria

The question of how many partitioning steps should be performed depends on the underlying research question. If the user is more interested in reducing the interaction-related heterogeneity as much as possible, they might split rather deeply, depending on the complexity of interactions learned by the model. However, this might lead to many regions that are more challenging to interpret. If the user is more interested in a small number of regions, they might prefer a shallow tree, thus reducing only the heterogeneity of the features that interact the most.

Here, we suggest the following stopping criteria to control the number of partitioning steps in GADGET: First, we could choose common hyperparameters of a decision tree, like the tree depth or the minimum number of observations per leaf node. Another option is to apply an early stop mechanism based on the interaction-related heterogeneity reduction—either in each split or in total. According to our proposed split-wise measure, a further split is only performed if the relative improvement of the split to be performed is at least

$\gamma \in [0, 1]$ times the total relative interaction-related heterogeneity reduction of the previous split: $\gamma \times \frac{\sum_{j \in S} (\mathcal{R}(\mathcal{A}_P, \mathbf{x}_j)) - \mathcal{I}(\hat{t}, \hat{z})}{\sum_{j \in S} (\mathcal{R}(\mathcal{X}, \mathbf{x}_j))}$. Another possibility is to stop splitting as soon as a pre-defined total reduction of heterogeneity (R_{Tot}^2) is reached. In general, it holds that the higher we choose γ and the lower we choose the threshold for R_{Tot}^2 , the fewer partitioning steps will be performed, and vice versa.

5 Significance Test for Global Feature Interactions

In addition to the hyperparameters for early stopping, there are two more hyperparameters in Algorithm 1 that must be specified—namely, the features of interest contained in S and the interacting (splitting) feature subset Z . Choosing the features to be contained in S and Z strongly depends on the underlying research question. If the user is interested in how a specific set of features (S) influences the model’s predictions depending on another user-defined feature set (Z), then S and Z are chosen based on domain knowledge. However, the user does not know which feature effects and interactions were inherently learned by the ML model. Thus, choosing S and Z based on domain knowledge does not guarantee that all interacting features are considered and that we can additively decompose the prediction function into univariate feature effects.

Thus, if our goal is to minimize feature interactions between all features to additively decompose the prediction function into mainly univariate effects, we can define $S = Z = \{1, \dots, p\}$. With that choice, we aim to reduce the overall interaction-related heterogeneity in all features (S), since we also consider all features to be possible interacting features (Z). However, this choice has two disadvantages. First, we must loop over all features and possible split points in each partitioning step, which may be slow in medium- or high-dimensional settings. This might also lead to less stable results, since only a few features might interact with each other, although many more features are considered for splitting. Second, if features are correlated, we might obtain spurious interactions (which we do not want to consider, since we are only interested in true interaction effects). Hence, to solely split according to feature interactions and only measure the interaction-related heterogeneity reduction, we must define beforehand the subset of features that actually interact. Since features interact with each other and all involved features will usually show heterogeneity in their local effects while being responsible for the heterogeneity of other involved features, we will usually choose $S = Z$.¹⁶ Thus, we will furthermore only use S as the globally interacting feature subset to be defined.

Since the H-Statistic (as defined in Section 2.4) is a global interaction measure, it could be used to define S by choosing all features with a high H-Statistic value. However, the question remains of which value is considered “high”. Furthermore, the H-Statistic is based on PDs. Thus, the interacting features are always chosen depending on the interaction quantification of PDs, which might differ from other feature effect methods (e.g., see the discussion of Shapley values versus ICE curves in Section 4.5). Since it is based on PDs, the H-Statistic might also suffer from detecting spurious interactions (Sorokina et al., 2008).

We introduce a new statistical permutation interaction test (PINT) that is inspired by the permutation importance (PIMP) algorithm of Altmann et al. (2010) to test for

16. Z might differ in the case of non-symmetrical interactions (see Section 7).

significant feature importance values. The goal of PINT (see Algorithm 2) is to define the feature subset S that contains all features that significantly interact with each other, w.r.t. a predefined significance level α and a chosen feature effect method. With the risk function defined in Eq. (11) and based on the chosen local feature effect method, we can quantify the interaction-related heterogeneity of each feature \mathbf{x}_j within the feature space \mathcal{X} . Due to correlations between features, the estimated heterogeneity might also include spurious interactions. Thus, we must define a null distribution to determine which heterogeneity is actually due to feature interactions (i.e., significant w.r.t. the null distribution) and which heterogeneity is due to other reasons, such as correlations or noise. This is achieved by permuting the target variable y (line 4 in Algorithm 2). With that, we break the association between the features and the target variable, but the underlying data structure remains. We refit the given ML model based on the data set $\tilde{\mathcal{D}}$ with the permuted target variable and calculate the respective risk $\tilde{\mathcal{R}}_j$ for each feature \mathbf{x}_j based on the chosen feature effect method h (lines 5-8 in Algorithm 2). This is repeated s times, producing s permuted risk values that represent the null distribution for the unpermuted risk value $\mathcal{R}(\mathcal{X}, \mathbf{x}_j)$ of the j -th feature. Then, we perform a statistical test based on the null hypothesis $H_0 : \mathcal{R}(\mathcal{X}, \mathbf{x}_j) \leq \tilde{\mathcal{R}}_j^{(s \cdot (1-\alpha))}$. Hence, if the unpermuted risk value is larger than the $(1-\alpha)$ -quantile of the null distribution, then the j -th feature is significant w.r.t. the defined α -level and belongs to the interacting feature subset S (lines 11-18 in Algorithm 2).

Algorithm 2: PINT

```

1: input: data set  $\mathcal{D}$ , prediction function  $\hat{f}$ , number of permutations  $s$ ,
   risk function  $\mathcal{R}$ , significance level  $\alpha$ 
2: output: feature subset  $S$ 
3: for  $k \in \{1, \dots, s\}$  do
4:   permute  $y$  of  $\mathcal{D}$  denoted by  $\tilde{y}^k$  and  $\tilde{\mathcal{D}}^k = \{\mathbf{x}, \tilde{y}^k\}$ 
5:   refit model on  $\tilde{\mathcal{D}}^k$  to obtain the prediction function  $\tilde{f}^k$ 
6:   for  $j \in \{1, \dots, p\}$  do
7:     calculate risk  $\tilde{\mathcal{R}}_j^{(k)} = \tilde{\mathcal{R}}^k(\mathcal{X}, \mathbf{x}_j)$  for  $j$ -the feature based on  $\tilde{\mathcal{D}}^k$  and  $\tilde{f}^k$ 
8:   end for
9: end for
10: for  $j \in \{1, \dots, p\}$  do
11:   a) calculate risk  $\mathcal{R}(\mathcal{X}, \mathbf{x}_j)$  for  $j$ -the feature based on  $\mathcal{D}$  and  $\hat{f}$ 
12:   b) sort  $\tilde{\mathcal{R}}_j$  in increasing order
13:   c) determine the  $(1 - \alpha)$ -quantile of permuted risk values  $z_j^{1-\alpha} = \tilde{\mathcal{R}}_j^{(s \cdot (1-\alpha))}$ 
14:   if  $\mathcal{R}(\mathcal{X}, \mathbf{x}_j) > z_j^{1-\alpha}$  then
15:      $j \in S$ 
16:   else
17:      $j \notin S$ 
18:   end if
19: end for
    
```

We illustrate the performance of PINT compared to the H-Statistic on an example which might be affected by spurious interactions. Therefore, we consider that $X_1, X_2, X_4 \sim$

$U(-1, 1)$ and $X_3 = X_2 + \epsilon$ with $\epsilon \sim N(0, 0.09)$. We draw $n = \{300, 500\}$ observations of these four random variables and assume the following relationship between \mathbf{y} and \mathbf{x} : $\mathbf{y} = \mathbf{x}_1 + \mathbf{x}_2 + \mathbf{x}_3 - 2\mathbf{x}_1\mathbf{x}_2$. Hence, \mathbf{x}_1 and \mathbf{x}_2 have a negative linear interaction effect, while \mathbf{x}_2 and \mathbf{x}_3 are highly linearly positively correlated but do not interact. Thus, there might be a spurious interaction between \mathbf{x}_1 and \mathbf{x}_3 . We calculate PINT and the H-Statistic for all features using a support vector machine (SVM) as the underlying ML model (with specifications defined in Section 6.3). We repeat the experiment 30 times. Figure 8 shows that for \mathbf{x}_1 and \mathbf{x}_2 , the PINT test is significant for almost all repetitions and effect methods, while it is never significant for features \mathbf{x}_3 and \mathbf{x}_4 w.r.t. a significance level of $\alpha = 0.05$. Hence, besides a few exceptions for ALE, the PINT algorithm returns the correct interacting feature subset $S = \{1, 2\}$. The H-Statistic shows that \mathbf{x}_1 interacts most with all other features, then \mathbf{x}_2 , followed by \mathbf{x}_3 and \mathbf{x}_4 in the rankings. Depending on which threshold is chosen, one would possibly include the non-interacting feature \mathbf{x}_3 in S , which shows over all repetitions values ranging from 0.1 to 0.2—possibly due to spurious interactions.

Hence, PINT not only allows to more clearly and (in this example) correctly define the subset S than the H-Statistic, but PINT also has the advantage that it can be used with any feature effect method that we use for GADGET. Thus, PINT can be applied according to the objective we want to minimize. This is analyzed in more detail in Section 6.

PINT also entails two hyperparameters α and s that must be specified. The significance level α can be chosen depending on the underlying research question. If we are only interested in a small set of very strong interactions, we choose α to be very small. If we want to find all (also small) interaction effects, we choose α to be larger. However, a larger significance level might also lead to detecting spurious interactions. The number of permutations s should be chosen to be as high as possible in order to obtain accurate results. However, since PINT must refit the model within each permutation, the computational burden increases with more permutations. One possible solution to address this trade-off for PIMP was proposed by Altmann et al. (2010), where the authors use a smaller number of permutations (e.g., 100) to approximate the empirical null distribution and then fit a theoretical distribution (e.g., normal, log-normal or gamma distribution) on the empirical distribution. Based on a Kolmogorov-Smirnov test, the theoretical distribution that best fits the empirical distribution is selected to approximate the null distribution. If the Kolmogorov-Smirnov test is not significant for any of the theoretical distributions, then the empirical distribution is used as the null distribution.¹⁷ This approach can similarly be applied for PINT. More suggestions to decrease the computational burden of PINT are provided in Appendix D.

6 Simulations

In this section, we analyze different hypotheses to (1) empirically validate that GADGET generally minimizes feature interactions and (2) show how different characteristics of the underlying data—such as correlations between features and different settings of the data-generating process—might influence GADGET, depending on the chosen feature effect method. The structure of the following sections and the concrete definition of the hypotheses is based on (2). However, the simulation examples themselves are designed in such a way

¹⁷. Note that Altmann et al. (2010) do not adjust for multiple testing, which can lead to false positives in higher dimensions (Molnar et al., 2022).

that we know the underlying ground-truth of feature interactions for each example. Thus, we are able to empirically validate that GADGET generally minimizes feature interactions.

6.1 Extrapolation

Hypothesis. For increasing correlation between features, due to extrapolation, we receive results that are less stable for methods using the marginal distribution for integration (especially PD, as shown in Section 3, but also SD) compared to methods using the conditional distribution (such as ALE). Note that in this context, “stability” refers to the ability of the different methods to find the correct split feature and split point in GADGET over various repetitions.

Experimental Setting. To address this hypothesis, we choose the (simple) simulation example of Section 3 and compare GADGET based on PD, ALE, and SD for four different correlation coefficients ρ_{13} between \mathbf{x}_1 and \mathbf{x}_3 —0, 0.4, 0.7, and 0.9. The data is generated as follows: Let $X_2, X_3 \sim \mathbb{U}(-1, 1)$ be independently distributed and $X_1 = c \cdot X_3 + (1 - c) \cdot Z$ with $Z \sim \mathbb{U}(-1, 1)$, where c takes values between 0 and 0.7, which correspond to the above-mentioned ρ_{13} values. The true underlying relationship is defined as before by $Y = 3X_1 \mathbb{1}_{X_3 > 0} - 3X_1 \mathbb{1}_{X_3 \leq 0} + X_3 + \epsilon$ with $\epsilon \sim \mathcal{N}(0, 0.09)$. We draw 1000 observations and fit a GAM with correctly specified main and interaction effects as well as an NN with the previously defined specifications to the data. We repeat the experiment 30 times.

We apply GADGET to each setting and model within each repetition using PD, ALE, and SD as feature effect methods. We consider all features as features of interest as well as potential interacting (split) features, meaning $S = Z = \{1, 2, 3\}$. As stopping criteria, we choose a maximum depth of 6, minimum number of observations per leaf of 40, and set the improvement parameter γ to 0.2.

Results. Figure 6 shows that independent of the model or correlation degree, \mathbf{x}_2 has (correctly) never been considered as split feature. For correlation strengths ρ_{13} between 0 and 0.7, \mathbf{x}_3 is always chosen as the only split feature, with I_3 taking values between 0.75 and 1 and, thus, reducing most of the interaction-related heterogeneity of all features with one split. Thus, for low to medium correlations, there are only minor differences between the various feature effect methods and models. However, the observed behavior changes substantially for $\rho_{13} = 0.9$. For the correctly-specified GAM, we still receive quite consistent results, apart from one repetition where \mathbf{x}_1 is chosen as the split feature when PD is used. In contrast, there is more variation of I_3 when the NN is considered as the underlying ML model, especially when SD is used. For SD, \mathbf{x}_1 is chosen once for splitting, and for PD, this is also the case for 30% of all repetitions (see Table 1). While using ALE, GADGET always correctly performs one split with regard to \mathbf{x}_3 . Additionally, GADGET performs a second split once when PD is used and 7 times when SD is used.

Thus, for a high correlation between features, we already observe in this very simple setting that the extrapolation problem influences the splitting within GADGET for effect methods based on marginal distributions, while methods based on conditional distributions such as ALE are less affected. This is particularly relevant for learners that model very locally (e.g., NNs) and thus, tend to have wiggly prediction functions and oscillate in ex-

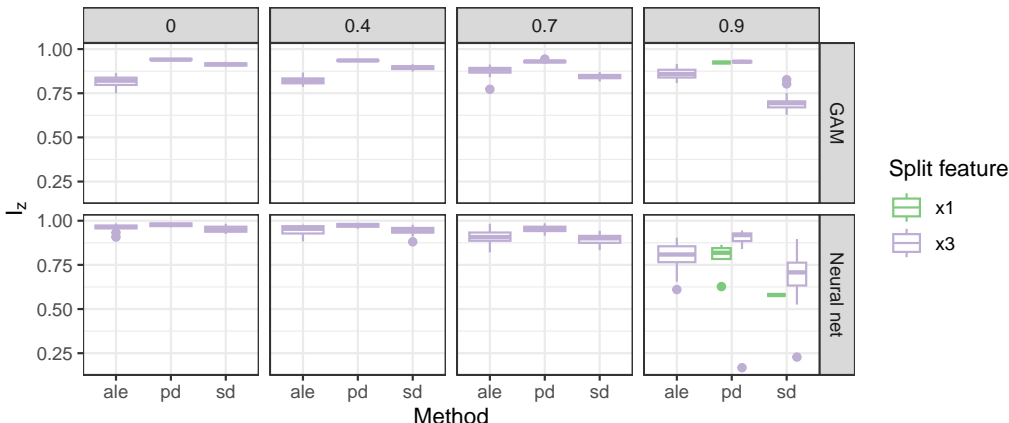


Figure 6: Boxplots showing the interaction-related heterogeneity reduction I_z per split feature over 30 repetitions when PD, ALE, or SD is used in GADGET. The columns show the results depending on the correlation between \mathbf{x}_1 and \mathbf{x}_3 , while the rows show the respective boxplots when GADGET is applied, based on the predictions of a correctly-specified GAM (upper) and of an NN (lower).

trapolating regions. This is also notable on the split value range, which increases for the NN in the case of high correlations for PD and SD but not for ALE (see Table 1).

		Split feature \mathbf{x}_3 in %			Split value range			MSE
Model	ρ_{13}	ALE	PD	SD	ALE	PD	SD	mean (sd)
GAM	0	1.00	1.00	1.00	0.10	0.10	0.12	0.329 (0.008)
GAM	0.4	1.00	1.00	1.00	0.13	0.10	0.10	0.201 (0.003)
GAM	0.7	1.00	1.00	1.00	0.09	0.10	0.09	0.137 (0.002)
GAM	0.9	1.00	0.97	1.00	0.11	0.11	0.12	0.107 (0.001)
NN	0	1.00	1.00	1.00	0.10	0.09	0.09	0.152 (0.018)
NN	0.4	1.00	1.00	1.00	0.08	0.08	0.07	0.124 (0.007)
NN	0.7	1.00	1.00	1.00	0.11	0.10	0.10	0.111 (0.005)
NN	0.9	1.00	0.70	0.97	0.10	0.19	0.15	0.104 (0.003)

Table 1: Overview of how often \mathbf{x}_3 was chosen as the first split feature over all 30 repetitions, including the respective split value range. The last column shows the test performance of the respective model by the mean (standard deviation) of the mean squared error (MSE).

6.2 Higher-Order Effects

Hypothesis. While SD puts less weight on interactions with increasing order, all interactions (independent of the order) receive the same weight in PD and ALE. Hence, when

GADGET-SD is used, we might not be able to detect interactions of high order—especially when the approximation without recalculation after each split is used (see Section 4.5). However, it should be more likely to detect these interactions with PD and ALE.

Experimental Setting. To investigate this hypothesis, we consider 5 features with $X_1 \sim \mathbb{U}(0, 1)$ and $X_2, X_3, X_4, X_5 \sim \mathbb{U}(-1, 1)$ and draw 1000 samples. The data-generating process is defined by a series of interactions between different features: $y = f(\mathbf{x}) + \epsilon$ with $f(\mathbf{x}) = \mathbf{x}_1 \cdot \mathbb{1}_{\mathbf{x}_3 \leq 0} \mathbb{1}_{\mathbf{x}_4 > 0} + 4\mathbf{x}_1 \cdot \mathbb{1}_{\mathbf{x}_3 \leq 0} \mathbb{1}_{\mathbf{x}_4 \leq 0} - \mathbf{x}_1 \cdot \mathbb{1}_{\mathbf{x}_3 > 0} \mathbb{1}_{\mathbf{x}_5 \leq 0} \mathbb{1}_{\mathbf{x}_2 > 0} - 3\mathbf{x}_1 \cdot \mathbb{1}_{\mathbf{x}_3 > 0} \mathbb{1}_{\mathbf{x}_5 \leq 0} \mathbb{1}_{\mathbf{x}_2 \leq 0} - 5\mathbf{x}_1 \cdot \mathbb{1}_{\mathbf{x}_3 > 0} \mathbb{1}_{\mathbf{x}_5 > 0}$ and $\epsilon \sim \mathcal{N}(0, 0.01 \cdot \sigma^2(f(\mathbf{x})))$. These interactions can be seen as one hierarchical structure between all features, where the slope of \mathbf{x}_1 depends on the subspace defined by the interacting features (see Figure 7).

We fit an xgboost (XGB) model with correctly-specified feature interactions and a random forest (RF) on the data set and apply GADGET using PD, ALE, SD with recalculation after each split, and SD without recalculation on each model. We repeat the experiment 30 times, where the XGB showed an average (standard deviation) MSE of 0.068(0.009) and the RF of 0.121(0.012) on a separate test set of the same distribution. For GADGET, we consider one feature of interest $S = 1$ and all other features as potential interacting features $Z = \{2, 3, 4, 5\}$. As stop criteria, we choose a maximum tree depth of 7, minimum number of observations of 40, and $\gamma = 0.1$. We can assume that if the underlying model learned the effects of the data-generating process correctly, GADGET must split as shown in Figure 7 to maximally reduce the interaction-related heterogeneity of \mathbf{x}_1 .

Results. For the first partitioning step, all methods used \mathbf{x}_3 as the first split feature in all repetitions. Table 2 shows that a second-level split was performed in only 10% of the repetitions for XGB when SD without recalculation is used within GADGET, while the second-level split frequency for all other methods is approximately 90%. A similar trend is observable when RF is used as underlying ML model but with higher variation in the relative frequencies, which might be due to different learned effects. If further splits for the second depth of the tree are performed, the correct split features \mathbf{x}_4 and \mathbf{x}_5 are always chosen by all methods, which shows that GADGET generally minimizes feature interactions (see Figure 7). Table 3 shows the same difference in relative frequencies between SD without recalculation and all other methods for the third-level splits as for the previous splits. This is confirmed by Table 4, which shows that while SD without recalculation demonstrates a high variation of final subspaces, the median number of subspaces is 2, indicating that this method stops after the first split (with \mathbf{x}_3). The other methods show a higher number of final subspaces; PD and SD with recalculation typically show the correct final number of subspaces (i.e., 5), while ALE tends to split slightly deeper.

To summarize, when SD without recalculation is used, the two-way interaction with \mathbf{x}_3 is primarily detected, while features of a third (\mathbf{x}_4 and \mathbf{x}_5) or fourth order (\mathbf{x}_2) interaction are rarely considered for splitting. By contrast, for most repetitions of the other three methods, we find that interactions of a higher order are also detected. This supports our hypothesis regarding higher-order effects and the theoretical differences of the considered feature effect methods.

Note that due to recalculating the Shapley values after each split, the order of interactions is reduced. For example, recalculating Shapley values in the subspace $\{\mathcal{X} | \mathbf{x}_3 \leq 0\}$ reduces the three-way interaction $\mathbf{x}_1 \cdot \mathbb{1}_{\mathbf{x}_3 \leq 0} \mathbb{1}_{\mathbf{x}_4 > 0}$ to the two-way interaction $\mathbf{x}_1 \cdot \mathbb{1}_{\mathbf{x}_4 > 0}$ and,

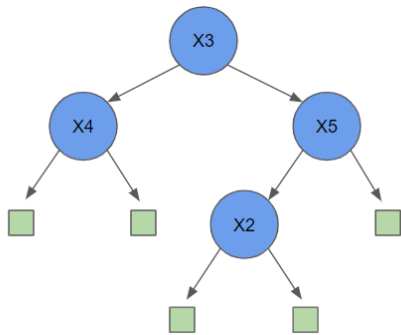


Figure 7: Explanation of the data-generating process. The green squares represent the 5 final subspaces which contain linear effects of feature \mathbf{x}_1 .

		$\mathcal{A}_l^{t,z}$		$\mathcal{A}_r^{t,z}$	
Model	Method	z	Freq.	z	Freq.
XGB	ALE	x4	0.93	x5	0.93
XGB	PD	x4	0.90	x5	0.90
XGB	SD_not_rc	x4	0.10	x5	0.10
XGB	SD_rc	x4	0.87	x5	0.87
RF	ALE	x4	0.80	x5	0.90
RF	PD	x4	0.63	x5	0.73
RF	SD_not_rc	x4	0.03	x5	0.13
RF	SD_rc	x4	0.73	x5	0.90

Table 2: Relative frequencies of splits by split feature z over 30 repetitions in the left $\mathcal{A}_l^{t,z}$ and right $\mathcal{A}_r^{t,z}$ subspaces after the first split when GADGET with ALE, PD, SD with recalculation (rc) and without recalculation (not_rc) is used.

thus, the weight of the interaction increases for the next split. Consequently, we receive similar results for these settings as we do for PD. However, one might consider that the recalculation can be computationally expensive.

Model	Method	z	Rel. Freq.
XGB	ALE	x2	0.93
XGB	PD	x2	0.90
XGB	SD_not_rc	x2	0.10
XGB	SD_rc	x2	0.87
RF	ALE	x2	0.83
RF	ALE	x4	0.03
RF	PD	x2	0.67
RF	SD_not_rc	x2	0.10
RF	SD_rc	x2	0.83

Table 3: Relative frequencies of splits by split feature z over all 30 repetitions in the subspace $\{\mathcal{X} | \mathbf{x}_3 > 0 \cap \mathbf{x}_5 \leq 0\}$ on third tree depth when GADGET is applied with ALE, PD, SD_not_rc and SD_rc.

		No. of Subspaces		
Model	Method	Min	Max	Med
XGB	ALE	3	15	7
XGB	PD	2	7	5
XGB	SD_not_rc	2	7	2
XGB	SD_rc	2	8	5
RF	ALE	3	16	9
RF	PD	2	11	5
RF	SD_not_rc	2	11	2
RF	SD_rc	3	12	5

Table 4: Minimum, maximum and median number of final subspaces over 30 repetitions after GADGET is applied with ALE, PD, SD_not_rc and SD_rc.

6.3 PINT vs. H-Statistic: Spurious Interactions

Hypothesis. When using PINT to pre-select $S = Z \subseteq \{1, \dots, p\}$, we are more likely to actually split according to feature interactions compared to when choosing all features ($S = Z = \{1, \dots, p\}$) or using the H-Statistic values for pre-selection, especially when potential spurious interactions are present.

Experimental Setting. We use the following simulation example described previously in Section 5: We consider four features with $X_1, X_2, X_4 \sim U(-1, 1)$ and $X_3 = X_2 + \epsilon$ with $\epsilon \sim N(0, 0.09)$. For 30 repetitions, we draw $n = \{300, 500\}$ observations and create the dependent variable, including a potential spurious interaction between \mathbf{x}_1 and \mathbf{x}_3 : $\mathbf{y} = \mathbf{x}_1 + \mathbf{x}_2 + \mathbf{x}_3 - 2\mathbf{x}_1\mathbf{x}_2$. For each sample size n and each repetition, we fit an SVM based on a radial basis function (RBF) kernel with cost parameter $C = 1$ and choose the inverse kernel width based on the data. We receive very similar model performance values—measured by the mean (standard deviation) of the MSE on a separate test set of size 100000 of the same distribution—of 0.028(0.010) and 0.027(0.010) for $n = 300$ and $n = 500$, respectively.

We calculate PINT using PD, ALE, and SD for each repetition and sample size with $s = 100$ and $\alpha = 0.05$ by approximating the null distribution as described in Section 5 and Altmann et al. (2010). We apply GADGET using PD, ALE, and SD with recalculation, where $S = Z$ is based on the feature subset chosen by PINT for the respective feature effect method. We compare these results with considering all features as features of interest and potential split features (i.e. $S = Z = \{1, \dots, p\}$). We use a maximum tree depth of 6, minimum number of observations of 40, and $\gamma = 0.15$ as stop criteria.

Results. The two left plots in Figure 8 show that \mathbf{x}_3 and \mathbf{x}_4 are always correctly identified as insignificant (according to the chosen α level), while the interacting features \mathbf{x}_1 and \mathbf{x}_2 are always significant and thus considered in S (apart from a few exceptions for ALE). The sample size does not seem to have a clear influence on PINT in this setting. The right plots in Figure 8 show that even the H-Statistic values of the non-influential and uncorrelated feature \mathbf{x}_4 are larger than 0 for both sample sizes. The H-Statistic values of \mathbf{x}_3 might support considering \mathbf{x}_3 in S , depending on which threshold is chosen. Since this choice is not clear for the H-Statistic, it is not very suitable as a pre-selection method for GADGET.

Figure 9 illustrates that we correctly only consider \mathbf{x}_1 and \mathbf{x}_2 when PINT is applied upfront, while GADGET also splits w.r.t. \mathbf{x}_3 for all settings and (in some cases) even w.r.t. \mathbf{x}_4 if PINT is not applied upfront. The influence of these two features seems to be higher for the smaller sample size according to I_z . Note that of the various effect methods used in GADGET, PD and SD attribute most of the heterogeneity reduction to \mathbf{x}_1 and a small part to \mathbf{x}_2 , while ALE attributes the heterogeneity more equally between the two split features. A possible explanation might be the correlation between \mathbf{x}_2 and \mathbf{x}_3 , which particularly affects the two methods based on marginal distributions (i.e., PD and SD). Furthermore, Table 5 shows that we tend to obtain shallower trees when we use PINT upfront, while we retain the level of heterogeneity reduction by obtaining similar R_j^2 values for the two interacting features \mathbf{x}_1 and \mathbf{x}_2 .

Thus, PINT reduces the number of features to consider in the interacting feature subset for GADGET depending on the regarded feature effect method. This leads to better results in GADGET in the sense that we only split w.r.t. truly interacting features defined by PINT and receive shallower (and thus, more interpretable) trees.

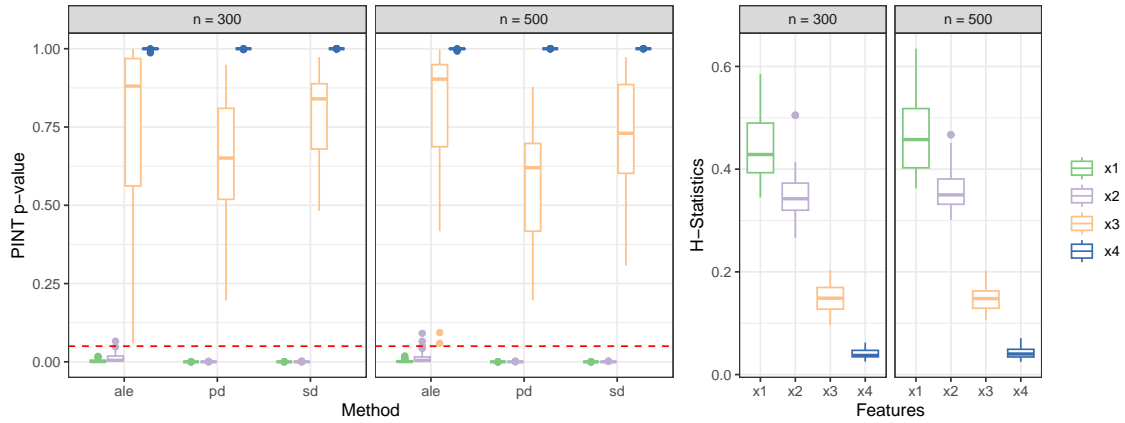


Figure 8: Boxplots showing the distribution of p-values of each feature for different sample sizes and effect methods over all repetitions when PINT is applied (left) and the distribution of feature-wise H-Statistic values for both sample sizes (right).

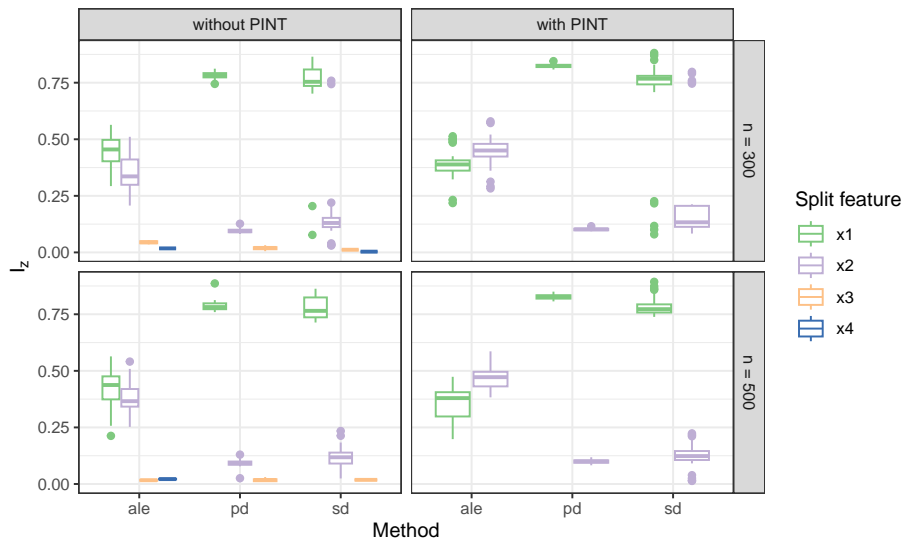


Figure 9: Boxplots showing the interaction-related heterogeneity reduction I_z per split feature over 30 repetitions when PD, ALE, or SD is used within GADGET. The rows show the results for the two different sample sizes, and the columns indicate if GADGET is used based on all features without using PINT upfront (left) or GADGET is used based on the feature subset resulting from PINT (right).

n	Method	PINT	R_j^2		Number of Subspaces		
			R_1^2 mean(sd)	R_2^2 mean(sd)	Min	Max	Median
300	ALE	no	0.83 (0.05)	0.83 (0.05)	4	10	7.50
300	ALE	yes	0.83 (0.07)	0.82 (0.05)	1	10	7.00
300	PD	no	0.94 (0.02)	0.84 (0.06)	2	7	4.00
300	PD	yes	0.92 (0.03)	0.80 (0.08)	2	5	3.00
300	SD	no	0.93 (0.04)	0.90 (0.05)	2	11	5.00
300	SD	yes	0.93 (0.04)	0.90 (0.05)	2	11	4.50
500	ALE	no	0.83 (0.04)	0.83 (0.06)	4	10	7.00
500	ALE	yes	0.86 (0.04)	0.82 (0.05)	1	11	6.50
500	PD	no	0.94 (0.03)	0.84 (0.06)	2	7	4.00
500	PD	yes	0.93 (0.03)	0.82 (0.08)	2	5	4.00
500	SD	no	0.93 (0.04)	0.90 (0.05)	2	11	5.00
500	SD	yes	0.93 (0.04)	0.90 (0.05)	2	9	5.00

Table 5: Interaction-related heterogeneity reduction per feature for \mathbf{x}_1 and \mathbf{x}_2 by mean (standard deviation) of R_j^2 and minimum, maximum and median number of final subspaces after applying GADGET based on different sample sizes, effect methods and with and without using PINT upfront.

7 Real-World Applications

In this section, we show the usefulness of our introduced methodology on two real-world application examples. These examples demonstrate that we can both obtain more insights about the learned effects and interactions of the underlying model as well as potentially be able to detect potential bias in the data or model.

COMPAS Data Set. Due to potential subjective judgement and a resulting bias in the decision-making process of the criminal justice system (Blair et al., 2004), ML models have been used to predict recidivism of defendants to provide a more objective guidance for judges. However, if the underlying training data is biased (e.g., different socioeconomic groups have been treated differently for the same crime in the past), the ML model might learn the underlying data bias and, due to its black-box nature, explanations for its decision-making process and a potential recourse are harder to achieve (Fisher et al., 2019).

We want to use GADGET here to obtain more insights in how different characteristics about the defendant and their criminal record influence the risk of recidivism within different subgroups and if “inadmissible” characteristics such as ethnicity or gender cause a different risk evaluation. For our analysis, we use a data set to predict the risk of violent recidivism gathered by ProPublica (Larson et al., 2016) from the Broward County Clerk’s Office, the Broward County Sheriff’s Office, and the Florida Department of Corrections, based on the commercial black-box model of Northpointe Inc. called the Correctional Offender Management Profiling for Alternative Sanctions (COMPAS) data set.

As Fisher et al. (2019), we choose the three admissible features (1) age of the defendant, (2) number of prior crimes, and (3) if the crime is considered a felony versus misdemeanor, and the two “inadmissible” features (1) ethnicity and (2) gender of the defendant. We use

the subset of African-American and Caucasian defendants and apply the data pre-processing steps suggested by ProPublica and applied in Fisher et al. (2019), which leaves us with 3373 defendants of the original pool of 4743 defendants. We consider a binary target variable indicating a high ($= 1$) or low ($= 0$) recidivism risk, which is based on a categorization of ProPublica. We perform our analysis on the full data set, using a tuned SVM.¹⁸

Since the features do not show high correlations, we use ICE and PD for our analysis.¹⁹ Figure 10 shows that the average predicted risk visibly decreases with age, while the predicted risk first steeply increases with the number of prior crimes until 10 and then slightly decreases for higher values. The PD values for the type of crime do not differ substantially. When considering the two “inadmissible” features, there is on average a slightly higher risk of recidivism for African-American versus Caucasian and female versus male defendants. For all features, we can observe highly differing local effects. In particular, the heterogeneous ICE curves for age and number of prior crimes indicate potential feature interactions.

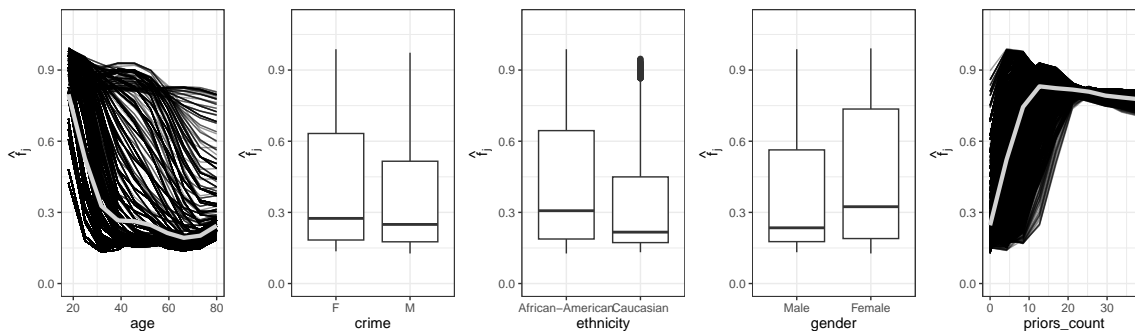


Figure 10: ICE and PD curves of considered features of the COMPAS application example.

We first apply PINT with PD to define our subset S for GADGET. To that end, we choose $s = 200$ and $\alpha = 0.05$ and approximate the null distribution using the procedure described in Section 5. All five features are significant w.r.t. the chosen significance level, and thus we choose $S = Z = \{age, crime, ethnicity, gender, priors_count\}$ for GADGET. We apply GADGET with a maximum depth of 3 and $\gamma = 0.15$. The effect plots for the four resulting regions are shown in Figure 11. GADGET performed the first split according to age and the splits on the second depth according to the number of prior crimes. The total interaction-related heterogeneity reduction is $R_{Tot}^2 = 0.86$. The highest heterogeneity reduction is given by age and number of prior crimes, which interact the most (see Figure 11). For defendants around 20 years old, the predicted risk is generally very high. However, for defendants with a small number of prior crimes, the predicted risk decreases very quickly with increasing age, reaching a low risk and remaining so for people older than 32. In contrast, for defendants with more than four prior crimes, the predicted risk decreases only slowly with increasing age. The regional feature effects of the number of prior crimes show that the interaction-related heterogeneity is small for the subgroup of younger people, while

18. More details on the model selection process can be found in Appendix E.

19. We received similar results by using SD instead of PD within GADGET, see Appendix E.

some heterogeneity still remains for defendants older than 32. Additionally, the interaction-related heterogeneity of the three binary features (ethnicity, gender, and crime severity) was reduced, indicating an interaction between each of them and age as well as the number of prior crimes. While the effect on the predicted risk only differs slightly between the categories of the three binary features for older defendants with a lower number of prior crimes and for younger defendants with a high number of prior crimes, greater differences were observed for the other two subgroups. The overall difference in predicted risk for the two inadmissible features of ethnicity and gender seems to be especially high for people older than 32 with a higher number of prior crimes as well as for people younger than 32 with a lower number of prior crimes.

Thus, our analysis has discovered a potentially learned bias regarding ethnicity and gender of the defendant, potentially resulting in more severe predicted risk of recidivism for some defendants than for others. Note that we applied GADGET on an ML model that is fitted on the COMPAS scores and not directly on COMPAS. Consequently, we are not able to draw conclusions about the learned effects of the underlying commercial black-box model. However, GADGET is model-agnostic and can be applied to any accessible black-box model.

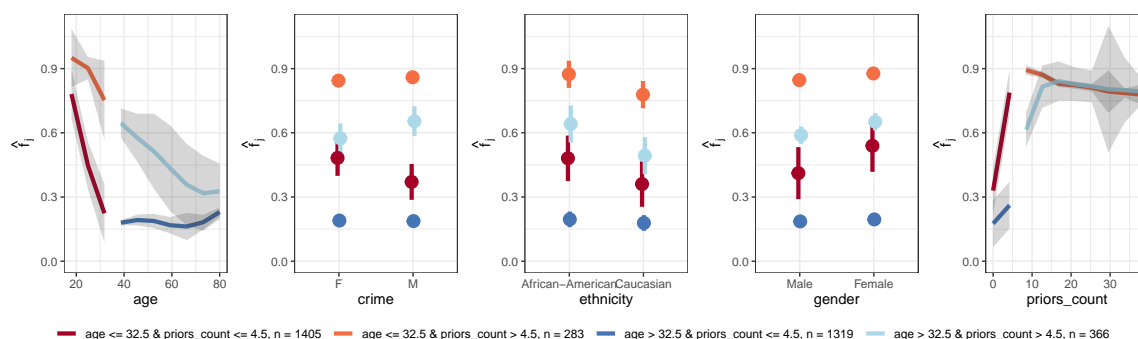


Figure 11: Regional PD plots for all features of the COMPAS application after applying GADGET. The grey areas of the numeric features and the error bars of the categorical features indicate the 95% interaction-related heterogeneity interval as defined in Section 4.3 and Appendix C.3.

Bikesharing Data Set. As a second application example, we choose the bikesharing data set provided in James et al. (2022). The target variable of this regression task is the hourly count of rented bikes for the years 2011 and 2012 in the Capital bikeshare system. The goal here is to predict the hourly rented bikes based on seasonal as well as weather information. We include ten features in our model for this prediction task: the day and hour the bike was rented, if the current day is a working day, the season, and the number of casual bikers. Weather-related features we included are: normalized temperature, perceived temperature, wind speed, humidity and the weather situation (categorical, e.g., clear).

We fit an RF on the data set and use the training data for our further analysis.²⁰

20. More details on the model selection process can be found in Appendix E.

Again, we first apply PINT (as done in the COMPAS example above) with $s = 200$ and $\alpha = 0.05$ on all features to define the interacting feature subset S for GADGET. Since some of the features—such as season, temperature, and perceived temperature—are correlated, we use ALE for our analysis. While the features hour and workingday are highly significant, the p-values of all other features are close to 1, indicating that only the heterogeneity of local effects for hour and workingday are caused by interactions. Hence, we define $S = Z = \{hr, workingday\}$ and apply GADGET with a maximum depth of 3 and $\gamma = 0.15$. GADGET splits once w.r.t. the binary feature workingday, which reduces the interaction-related heterogeneity of the two features by $R_{Tot}^2 = 0.88$. The middle plots of Figure 12 show the regional ALE plots after applying GADGET. High peaks are prominently visible on working days during rush hours, while there is a drop during noon and afternoon hours. However, on non-working days, the trend is the opposite. This interaction is not visible in the global ALE plot of the feature hour (left plot).

The interaction-related heterogeneity of the feature hour is reduced compared to the global plot, although there is still some variation apparent for working days. From a domain perspective, we might also consider an interaction of the temperature with hour and working day (as done in Hiabu et al., 2023). Thus, we include temperature in feature subsets S and Z and apply GADGET again with the same settings as described above. The feature workingday governs the first split. However, for the region of working days, GADGET splits again according to temperature, as shown in the right plot of Figure 12. While the interaction-related heterogeneity of feature temperature was barely reduced within GADGET ($R_j^2 = 0.03$)—which supports the results of PINT—using temperature in the subset of splitting features Z further reduced the interaction-related heterogeneity of hour by 15%. Thus, feature interactions can be asymmetric, and extending Z based on domain knowledge might be a valid option in some cases.

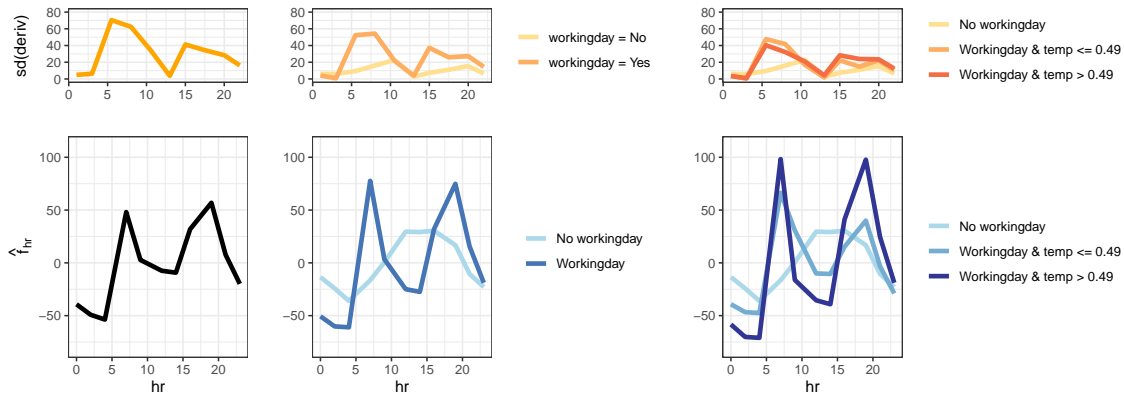


Figure 12: Global (left), regional ALE plots after applying GADGET for feature hour when $S = Z = \{hr, workingday\}$ (middle) and when $S = Z = \{hr, workingday, temp\}$ (right) of the bikesharing application. The upper plots show the interaction-related heterogeneity as defined in Section 4.4 and Appendix C.3.

8 Conclusion and Discussion

We introduced the new framework GADGET, which partitions the feature space into interpretable and distinct regions such that feature interactions of any subset of features are minimized. This allows to decompose joint effects into features’ main effects within the found regions. GADGET can be used with any feature effect method that satisfies the *local decomposability* axiom (Axiom 1). We showed applicability to the well-known global feature effect methods—namely PD, ALE, and SD—and provide respective estimates and visualizations for regional feature effects and interaction-related heterogeneity. Furthermore, we introduced different measures to quantify and analyze feature interactions by the reduction of interaction-related heterogeneity within GADGET. To define the interacting feature subset, we introduced PINT, a novel permutation-based significance test to detect global feature interactions that is applicable to any feature effect method used within GADGET.

Our experiments showed that PINT is often able to detect the true interacting feature subset in the presence of spurious interactions and that the pre-selection thus leads to more meaningful and interpretable results in GADGET. Moreover, considering feature effect methods within GADGET that are based on conditional distribution tend to lead to more stable results compared to considering feature effect methods based on marginal distribution when features are highly correlated. Furthermore, due to a different weighting scheme in the decomposition of Shapely values compared to the other considered feature effect methods, higher-order terms are less likely to be detected by GADGET, especially if Shapley values are not recalculated after each partitioning step. This approach might be computationally expensive, which can be seen as a possible limitation. However, recent research has focused on fast approximation techniques of Shapley values (e.g., Lundberg and Lee, 2017; Jethani et al., 2021; Lundberg et al., 2020; Chau et al., 2022) and may offer solutions to overcoming this limitation.

In general, our proposed method works well if learned feature interactions are not overly local and if observations can be grouped based on feature interactions such that local feature effects within the groups are homogeneous and, at the same time, show heterogeneous feature effects between different groups. With that, we can avoid an aggregation bias of global feature effect methods, obtain more insights into the learned effects, and may detect potential biases within different subgroups (as illustrated in Section 7). One of the real-world examples also showed that the frequently-made assumption of symmetric feature interactions (e.g., in Shapley values) is not always the case (see also Masoomi et al., 2023, for research on asymmetrical feature interactions). Thus, including domain knowledge to define the interacting feature subset Z might sometimes be meaningful.

Acknowledgments and Disclosure of Funding

This work has been partially supported by the Bavarian Ministry of Economic Affairs, Regional Development and Energy as part of the program “Bayerischen Verbundförderprogramms (BayVFP) – Förderlinie Digitalisierung – Förderbereich Informations- und Kommunikationstechnik” under the grant DIK-2106-0007 // DIK0260/02. The authors of this work take full responsibility for its content.

Appendix A. Details on M Plot

The M plot for feature \mathbf{x}_j at feature value x_j is defined as the marginal effect of feature \mathbf{x}_j using the conditional distribution (compared to the marginal distribution used in PD functions):

$$f_j^M(x_j) = \mathbb{E}[\hat{f}(X_j, X_{-j})|X_j = x_j] = \int \hat{f}(x_j, \mathbf{x}_{-j})d\mathbb{P}(\mathbf{x}_{-j}|x_j).$$

Hence, similar to PD plots, the local feature effect of M plots are also predictions at a specific feature value of \mathbf{x}_j but w.r.t. the conditional distribution $\mathbb{P}(\mathbf{x}_{-j}|x_j)$. Therefore, M plots can be seen as an average over ICE curves, which are restricted based on the given correlation structure. This leads to the inclusion of the feature effects of correlated features, as illustrated in the following example.

We draw 1000 samples of two multivariate normally distributed random variables X_1 and X_2 with $\mu_1 = \mu_2 = 0$, $\sigma_1 = \sigma_2 = 1$ and $\sigma_{12} = 0.9$. The true data-generating process is given by $y = -\mathbf{x}_1 + 2\mathbf{x}_2 + \epsilon$ with $\epsilon \sim \mathcal{N}(0, 0.2)$. We train a linear model on the given data set. Based on the learned effects of the linear model, we would assume that the feature \mathbf{x}_1 has a negative influence on the predictions, as shown by the PD plot in Figure 13 (left). On the other hand, the M Plot accounts for the effect of the correlated feature \mathbf{x}_2 , which has a positive effect and (in absolute terms) a higher influence on the predictions than \mathbf{x}_1 , which leads to a positive slope in the right plot of Figure 13.

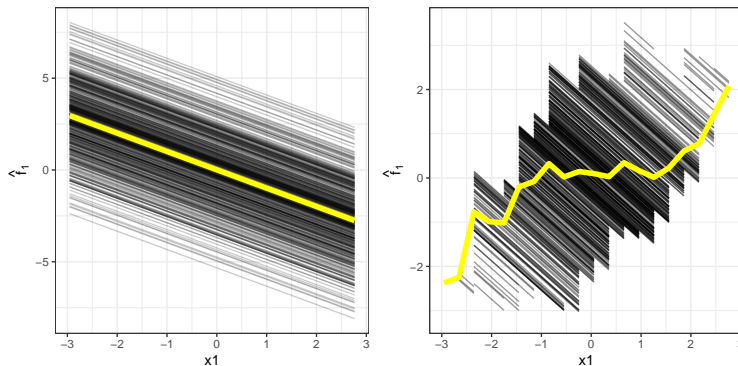


Figure 13: PD plot (left) and M Plot (right) for feature \mathbf{x}_1 .

Appendix B. Theoretical Evidence of GADGET

In this appendix, we provide the proofs for the theorems and the corollary of Section 4.2. Furthermore, we show the applicability of the feature effect methods PD, ALE, and SD within the GADGET algorithm by defining respective local feature effect functions that fulfill Axiom 1.

B.1 Proof of Theorem 2

Proof Sketch If the function $\hat{f}(\mathbf{x})$ can be decomposed as in Eq. (1) and if Axiom 1 holds for the local feature effect function h , then the main effect of feature \mathbf{x}_j at x_j is cancelled

out within the loss function in Eq. (10). Thus, the loss function measures the interaction-related heterogeneity of feature \mathbf{x}_j at x_j , since the variability of local effects in the subspace \mathcal{A}_g are only based on feature interactions between the j -th feature and features in $-j$.

Proof

$$\begin{aligned}
 \mathcal{L}(\mathcal{A}_g, x_j) &= \sum_{i:\mathbf{x}^{(i)} \in \mathcal{A}_g} \left(h(x_j, \mathbf{x}_{-j}^{(i)}) - \mathbb{E}[h(x_j, X_{-j}) | \mathcal{A}_g] \right)^2 \\
 &= \sum_{i:\mathbf{x}^{(i)} \in \mathcal{A}_g} \left(g_j(x_j) + \sum_{k=1}^{p-1} \sum_{\substack{W \subseteq -j, \\ |W|=k}} g_{W \cup j}(x_j, \mathbf{x}_W^{(i)}) - \mathbb{E}[g_j(x_j) + \sum_{k=1}^{p-1} \sum_{\substack{W \subseteq -j, \\ |W|=k}} g_{W \cup j}(x_j, X_W) | \mathcal{A}_g] \right)^2 \\
 &= \sum_{i:\mathbf{x}^{(i)} \in \mathcal{A}_g} \left(\sum_{k=1}^{p-1} \sum_{\substack{W \subseteq -j, \\ |W|=k}} g_{W \cup j}(x_j, \mathbf{x}_W^{(i)}) - \mathbb{E}[g_{W \cup j}(x_j, X_W) | \mathcal{A}_g] \right)^2
 \end{aligned}$$

■

B.2 Proof of Theorem 3

Proof Sketch We show in two steps that the objective in Algorithm 1 minimizes interaction-related heterogeneity between features in S and Z . First, if the function $\hat{f}(\mathbf{x})$ can be decomposed as in Eq. (1) and if Axiom 1 holds for the local feature effect function h , then we can show (based on Theorem 2) that the objective $\mathcal{I}(t, z)$ in Algorithm 1 is defined by feature interactions between each feature $j \in S$ and features in $-j$. Second, since we only consider features in Z for splitting and thus minimize the interaction-related heterogeneity of features in S , we can show that feature interactions between features in S and features in $-Z$ are independent of the partitioning in Algorithm 1 (if all features contained in Z and all features in $-Z$ are pair-wise independent) and thus are not directly minimized in the objective $\mathcal{I}(t, z)$.

Proof

$$\begin{aligned}
 \mathcal{I}(t, z) &= \sum_{j \in S} \sum_{b \in \{l, r\}} (\mathcal{R}(\mathcal{A}_b^{t, z}, \mathbf{x}_j)) \\
 &\stackrel{\text{Eq. (11)}}{=} \sum_{j \in S} \sum_{b \in \{l, r\}} \left(\sum_{\substack{k: k \in \{1, \dots, m\} \\ \wedge x_j^{(k)} \in \mathcal{A}_l^{t, z}}} \mathcal{L}(\mathcal{A}_b^{t, z}, x_j^{(k)}) \right) \\
 &\stackrel{\text{Eq. (10)}}{=} \sum_{j \in S} \sum_{b \in \{l, r\}} \sum_{\substack{k: k \in \{1, \dots, m\} \\ \wedge x_j^{(k)} \in \mathcal{A}_b^{t, z}}} \sum_{i:\mathbf{x}^{(i)} \in \mathcal{A}_b^{t, z}} \left(h(x_j^{(k)}, \mathbf{x}_{-j}^{(i)}) - \mathbb{E}[h(x_j^{(k)}, X_{-j}) | \mathcal{A}_b^{t, z}] \right)^2 \\
 &\stackrel{\text{T. 2}}{=} \sum_{j \in S} \sum_{b \in \{l, r\}} \sum_{\substack{k: k \in \{1, \dots, m\} \\ \wedge x_j^{(k)} \in \mathcal{A}_b^{t, z}}} \sum_{i:\mathbf{x}^{(i)} \in \mathcal{A}_b^{t, z}} \left(\sum_{l=1}^{p-1} \sum_{\substack{W \subseteq -j, \\ |W|=l}} g_{W \cup j}(x_j, \mathbf{x}_W^{(i)}) - \mathbb{E}[g_{W \cup j}(x_j, X_W) | \mathcal{A}_b^{t, z}] \right)^2
 \end{aligned}$$

The objective function $\mathcal{I}(t, z)$ is defined by the interaction-related heterogeneity between all features $j \in S \subseteq \{1, \dots, p\}$ and features in $-j$ for the sum of the left and right subspace $\mathcal{A}_l^{t,z}$ and $\mathcal{A}_r^{t,z}$. Since the aim is to minimize this term, we choose the split feature $z \in Z \subseteq \{1, \dots, p\}$ and split point t , which minimizes the sum of the risk values. However, since we only split w.r.t. features in Z and not w.r.t. feature in $-Z$, the objective focuses on minimizing the heterogeneity between features in S and features in Z , while interactions between features in S and features in $-Z$ are generally not minimized, since the heterogeneity is independent of the subspace $\mathcal{A}_b^{t,z}$.²¹ This can be shown by decomposing the risk function for features $j \in S$ into interaction effects between feature \mathbf{x}_j and features in Z (first term), interaction effects between feature \mathbf{x}_j and features in $-j$ with at least one feature of the subset Z and at least one feature of the subset $-Z$ (second term), and interaction effects between feature \mathbf{x}_j and features in $-Z$ (third term):

$$\begin{aligned} \mathcal{R}(\mathcal{A}_b^{t,z}, \mathbf{x}_j) &= \sum_{\substack{k:k \in \{1, \dots, m\} \\ \wedge \mathbf{x}_j^{(k)} \in \mathcal{A}_b^{t,z}}} \sum_{i:\mathbf{x}^{(i)} \in \mathcal{A}_b^{t,z}} \left(\sum_{l=1}^{p-1} \sum_{\substack{W \subseteq -j, \\ |W|=l}} g_{W \cup j}(x_j, \mathbf{x}_W^{(i)}) - \mathbb{E}[g_{W \cup j}(x_j, X_W) | \mathcal{A}_b^{t,z}] \right)^2 \\ &= \sum_{\substack{k:k \in \{1, \dots, m\} \\ \wedge \mathbf{x}_j^{(k)} \in \mathcal{A}_b^{t,z}}} \sum_{i:\mathbf{x}^{(i)} \in \mathcal{A}_b^{t,z}} \left(\left(\sum_{l=1}^{|Z \setminus j|} \sum_{\substack{Z_l \subseteq Z \setminus j, \\ |Z_l|=l}} g_{Z_l \cup j}(x_j, \mathbf{x}_{Z_l}^{(i)}) - \mathbb{E}[g_{Z_l \cup j}(x_j, X_{Z_l}) | \mathcal{A}_b^{t,z}] \right) \right. \\ &\quad + \left. \left(\sum_{l=2}^{p-1} \sum_{\substack{W \subseteq -j \\ \wedge \exists Z_l \subseteq Z \setminus j: Z_l \subset W \\ \wedge \exists -Z_l \subseteq -Z \setminus j: -Z_l \subset W, \\ |W|=l}} g_{W \cup j}(x_j, \mathbf{x}_{Z_l}^{(i)}, \mathbf{x}_{-Z_l}^{(i)}) - \mathbb{E}[g_{W \cup j}(x_j, X_{Z_l}, X_{-Z_l}) | \mathcal{A}_b^{t,z}] \right) \right. \\ &\quad \left. + \left(\sum_{l=1}^{|-Z \setminus j|} \sum_{\substack{-Z_l \subseteq -Z \setminus j, \\ |-Z_l|=l}} g_{-Z_l \cup j}(x_j, \mathbf{x}_{-Z_l}^{(i)}) - \mathbb{E}[g_{-Z_l \cup j}(x_j, X_{-Z_l}) | \mathcal{A}_b^{t,z}] \right) \right)^2 \end{aligned}$$

While the first two terms contain feature interactions between j and features in Z , the last term does not. Furthermore, this term is (at least, in an uncorrelated setting) independent of the regarded subspace $\mathcal{A}_b^{t,z}$ and, thus, is not directly minimized by the given objective:

$$\left(\sum_{l=1}^{|-Z \setminus j|} \sum_{\substack{-Z_l \subseteq -Z \setminus j, \\ |-Z_l|=l}} g_{-Z_l \cup j}(x_j, \mathbf{x}_{-Z_l}^{(i)}) - \mathbb{E}[g_{-Z_l \cup j}(x_j, X_{-Z_l}) | \mathcal{A}_b^{t,z}] \right) \perp\!\!\!\perp \mathcal{A}_b^{t,z}$$

since $\mathbb{E}[g_{-Z_l \cup j}(x_j, X_{-Z_l}) | \mathcal{A}_b^{t,z}] = \mathbb{E}[g_{-Z_l \cup j}(x_j, X_{-Z_l})]$. ■

B.3 Proof of Corollary 4

Proof Sketch Based on Theorem 3, we can show that the theoretical minimum of the objective is $\mathcal{I}(t^*, z^*) = 0$ if no feature in S interacts with any feature in $-Z$. In the following

21. This might be different if features in Z and $-Z$ are highly correlated.

proof, we apply the same decomposition of the risk function $\mathcal{R}(\mathcal{A}_b^{t,z}, \mathbf{x}_j)$, as done in the proof of Theorem 3. Since we assume that no feature in S interacts with any feature in $-Z$, the second and third term—which contain interactions between these two feature subsets—are zero. Hence, the risk function is only defined by feature interactions between features in S and Z , which are minimized by the objective in Algorithm 1.

Proof If the feature subset Z contains all features interacting with features in S , and hence no feature in $-Z$ interacts with any feature in S , then (w.r.t. the decomposition of the risk function in the proof of Theorem 3) the risk function for feature \mathbf{x}_j within a subspace $\mathcal{A}_b^{t,z}$ reduces to the variance of feature interactions between feature \mathbf{x}_j and features in Z :

$$\begin{aligned}
 \mathcal{R}(\mathcal{A}_b^{t,z}, \mathbf{x}_j) &= \sum_{\substack{k: k \in \{1, \dots, m\} \\ \wedge \mathbf{x}_j^{(k)} \in \mathcal{A}_b^{t,z}}} \sum_{i: \mathbf{x}^{(i)} \in \mathcal{A}_b^{t,z}} \left(\left(\sum_{l=1}^{|Z \setminus j|} \sum_{\substack{Z_l \subseteq Z \setminus j, \\ |Z_l|=l}} g_{Z_l \cup j}(x_j, \mathbf{x}_{Z_l}^{(i)}) - \mathbb{E}[g_{Z_l \cup j}(x_j, X_{Z_l}) | \mathcal{A}_b^{t,z}] \right) \right. \\
 &+ \left(\sum_{l=2}^{p-1} \sum_{\substack{W \subseteq -j \\ \wedge \exists Z_l \subseteq Z \setminus j: Z_l \subseteq W \\ \wedge \exists -Z_l \subseteq -Z \setminus j: -Z_l \subseteq W, \\ |W|=l}} \underbrace{g_{W \cup j}(x_j, \mathbf{x}_{Z_l}^{(i)}, \mathbf{x}_{-Z_l}^{(i)}) - \mathbb{E}[g_{W \cup j}(x_j, X_{Z_l}, X_{-Z_l}) | \mathcal{A}_b^{t,z}]}_{=0} \right) \\
 &+ \left. \left(\sum_{l=1}^{|-Z \setminus j|} \sum_{\substack{-Z_l \subseteq -Z \setminus j, \\ |-Z_l|=l}} \underbrace{g_{-Z_l \cup j}(x_j, \mathbf{x}_{-Z_l}^{(i)}) - \mathbb{E}[g_{-Z_l \cup j}(x_j, X_{-Z_l}) | \mathcal{A}_b^{t,z}]}_{=0} \right) \right)^2 \\
 &= \sum_{\substack{k: k \in \{1, \dots, m\} \\ \wedge \mathbf{x}_j^{(k)} \in \mathcal{A}_b^{t,z}}} \sum_{i: \mathbf{x}^{(i)} \in \mathcal{A}_b^{t,z}} \left(\sum_{l=1}^{|Z \setminus j|} \sum_{\substack{Z_l \subseteq Z \setminus j, \\ |Z_l|=l}} g_{Z_l \cup j}(x_j, \mathbf{x}_{Z_l}^{(i)}) - \mathbb{E}[g_{Z_l \cup j}(x_j, X_{Z_l}) | \mathcal{A}_b^{t,z}] \right)^2
 \end{aligned}$$

Since the objective is defined such that it minimizes these interactions for all $j \in S$ by splitting the feature space w.r.t. features in Z , we can split deep enough to achieve $g_{Z_l \cup j}(x_j, \mathbf{x}_{Z_l}^{(i)}) = \mathbb{E}[g_{Z_l \cup j}(x_j, X_{Z_l}) | \mathcal{A}_b^{t,z}]$ for all terms within the sums of the risk function and for all $j \in S$. In other words, the individual interaction effect is equal to the expected interaction effect within a subspace, and thus the theoretical minimum of the objective is $\mathcal{I}(t^*, z^*) = 0$. \blacksquare

B.4 Applicability of PD within GADGET

Here, we show how h must be defined to fulfill Axiom 1 defined in Section 4.2 for the feature effect method PD.

Local Decomposition: The local feature effect method used in PDs are ICE curves. The i -th ICE curve of feature \mathbf{x}_j can be decomposed as follows:

$$\begin{aligned}
 \hat{f}(\mathbf{x}_j, \mathbf{x}_{-j}^{(i)}) &= \underbrace{g_0}_{\text{constant term}} + \underbrace{g_j(\mathbf{x}_j)}_{\text{main effect of } \mathbf{x}_j} + \underbrace{\sum_{k \in -j} g_k(\mathbf{x}_k^{(i)})}_{\substack{\text{main effect of all other} \\ \text{features in } -j \text{ for observation } i}} \\
 &+ \underbrace{\sum_{k=1}^{p-1} \sum_{\substack{W \subseteq -j, \\ |W|=k}} g_{W \cup \{j\}}(\mathbf{x}_j, \mathbf{x}_W^{(i)})}_{(k+1)\text{-order interaction between} \\ &\quad \mathbf{x}_j \text{ and features in } -j \text{ for observation } i} + \underbrace{\sum_{k=2}^{p-1} \sum_{\substack{W \subseteq -j, \\ |W|=k}} g_W(\mathbf{x}_W^{(i)})}_{k\text{-order interaction between} \\ &\quad \text{features in } -j \text{ for observation } i}
 \end{aligned}$$

However, this decomposition of the local feature effect of \mathbf{x}_j contains not only feature effects that depend on \mathbf{x}_j , but also other effects (e.g., i -th main effects of features in $-j$), and thus Axiom 1 is not fulfilled by ICE curves. However, by mean-centering ICE curves, constant and feature effects independent of \mathbf{x}_j are cancelled out, and thus $\hat{f}^c(\mathbf{x}_j, \mathbf{x}_{-j}^{(i)})$ can be decomposed into the mean-centered main effect of \mathbf{x}_j and the i -th mean-centered interaction effect between \mathbf{x}_j and features in $-j$. Hence, the mean-centered ICE of feature \mathbf{x}_j at x_j can be decomposed as follows:

$$\begin{aligned}
 \hat{f}^c(x_j, \mathbf{x}_{-j}^{(i)}) &= \hat{f}(x_j, \mathbf{x}_{-j}^{(i)}) - \mathbb{E}[\hat{f}(X_j, \mathbf{x}_{-j}^{(i)})] \\
 &= g_0 + g_j(x_j) + \sum_{k \in -j} g_k(\mathbf{x}_k^{(i)}) + \sum_{k=1}^{p-1} \sum_{\substack{W \subseteq -j, \\ |W|=k}} g_{W \cup \{j\}}(x_j, \mathbf{x}_W^{(i)}) + \sum_{k=2}^{p-1} \sum_{\substack{W \subseteq -j, \\ |W|=k}} g_W(\mathbf{x}_W^{(i)}) \\
 &- g_0 - E[g_j(X_j)] - \sum_{k \in -j} g_k(\mathbf{x}_k^{(i)}) - E \left[\sum_{k=1}^{p-1} \sum_{\substack{W \subseteq -j, \\ |W|=k}} g_{W \cup \{j\}}(X_j, \mathbf{x}_W^{(i)}) \right] - \sum_{k=2}^{p-1} \sum_{\substack{W \subseteq -j, \\ |W|=k}} g_W(\mathbf{x}_W^{(i)}) \\
 &= g_j(x_j) - E[g_j(X_j)] + \sum_{k=1}^{p-1} \sum_{\substack{W \subseteq -j, \\ |W|=k}} g_{W \cup \{j\}}(x_j, \mathbf{x}_W^{(i)}) - E \left[\sum_{k=1}^{p-1} \sum_{\substack{W \subseteq -j, \\ |W|=k}} g_{W \cup \{j\}}(X_j, \mathbf{x}_W^{(i)}) \right] \\
 &= \underbrace{g_j^c(x_j)}_{\substack{\text{mean-centered} \\ \text{main effect of } \mathbf{x}_j}} + \underbrace{\sum_{k=1}^{p-1} \sum_{\substack{W \subseteq -j, \\ |W|=k}} g_{W \cup \{j\}}^c(x_j, \mathbf{x}_W^{(i)})}_{\substack{\text{mean-centered interaction effect of} \\ \mathbf{x}_j \text{ with } \mathbf{x}_{-j}^{(i)}}}
 \end{aligned}$$

Thus, Axiom 1 is satisfied by mean-centered ICE curves and can be used as local feature effect h within GADGET. Following from that, the mean-centered PD for feature \mathbf{x}_j at x_j can be decomposed by:

$$f_j^{PD,c}(x_j) = \mathbb{E}[\hat{f}^c(x_j, X_{-j})] = g_j^c(x_j) + \sum_{k=1}^{p-1} \sum_{\substack{W \subseteq -j, \\ |W|=k}} E \left[g_{W \cup \{j\}}^c(x_j, X_W) \right],$$

which is the mean-centered main effect of feature \mathbf{x}_j and the expected mean-centered interaction effect with feature \mathbf{x}_j at feature value x_j . Based on these decompositions and for

$h = \hat{f}^c(x_j, \mathbf{x}_{-j}^{(i)})$, we can show that the loss function only depends on the feature interaction effect between the j -th feature and features in $-j$ (Theorem 2):

$$\begin{aligned}
 \mathcal{L}^{PD}(\mathcal{A}_g, x_j) &= \sum_{i: \mathbf{x}^{(i)} \in \mathcal{A}_g} \left(\hat{f}^c(x_j, \mathbf{x}_{-j}^{(i)}) - \mathbb{E}[\hat{f}^c(x_j, X_{-j}) | \mathcal{A}_g] \right)^2 \\
 &= \sum_{i: \mathbf{x}^{(i)} \in \mathcal{A}_g} \left(g_j^c(x_j) + \sum_{k=1}^{p-1} \sum_{\substack{W \subseteq -j, \\ |W|=k}} g_{W \cup \{j\}}^c(x_j, \mathbf{x}_W^{(i)}) \right. \\
 &\quad \left. - g_j^c(x_j) - \sum_{k=1}^{p-1} \sum_{\substack{W \subseteq -j, \\ |W|=k}} \mathbb{E}[g_{W \cup \{j\}}^c(x_j, X_W) | \mathcal{A}_g] \right)^2 \\
 &= \sum_{i: \mathbf{x}^{(i)} \in \mathcal{A}_g} \left(\sum_{k=1}^{p-1} \sum_{\substack{W \subseteq -j, \\ |W|=k}} g_{W \cup \{j\}}^c(x_j, \mathbf{x}_W^{(i)}) - \mathbb{E}[g_{W \cup \{j\}}^c(x_j, X_W) | \mathcal{A}_g] \right)^2
 \end{aligned}$$

REPID as special case of GADGET. The objective function $\mathcal{I}(t, z)$ in Algorithm 1 for $h = \hat{f}^c(x_j, \mathbf{x}_{-j}^{(i)})$ is defined by the above loss function $\mathcal{L}^{PD}(\mathcal{A}_g, x_j)$ as follows:

$$\mathcal{I}(t, z) = \sum_{j \in S} \sum_{g \in \{l, r\}} \sum_{k: k \in \{1, \dots, m\} \wedge \mathbf{x}_j^{(k)} \in \mathcal{A}_g} \mathcal{L}^{PD}(\mathcal{A}_g, \mathbf{x}_j^{(k)})$$

For the special case where we consider one feature of interest that we want to visualize ($S = j$) and all other features as possible split features ($Z = -j$), the objective function of GADGET reduces to:

$$\mathcal{I}(t, z) = \sum_{g \in \{l, r\}} \sum_{k=1}^m \mathcal{L}^{PD}(\mathcal{A}_g, \mathbf{x}_j^{(k)}),$$

which is the same objective used within REPID. Thus, for the special case where we choose mean-centered ICE curves as local feature effect method and $S = j$ and $Z = -j$, GADGET is equivalent to REPID.

B.5 Applicability of ALE Within GADGET

Here, we show the fulfillment of Axiom 1 defined in Section 4.2 for the underlying local feature effect function in ALE.

Local Decomposition: The local feature effect method used in ALE is the partial derivative of the prediction function at $\mathbf{x}_j = x_j$. Thus, we define the local feature effect function h by $h(x_j, \mathbf{x}_{-j}^{(i)}) := \frac{\partial \hat{f}(x_j, \mathbf{x}_{-j}^{(i)})}{\partial x_j}$. We can decompose h such that it only depends on main and interaction effects of and with feature \mathbf{x}_j :

$$\begin{aligned} \frac{\partial \hat{f}(x_j, \mathbf{x}_{-j}^{(i)})}{\partial x_j} &= \frac{\partial \left(g_0 + \sum_{j=1}^p g_j(x_j) + \sum_{j \neq k} g_{jk}(x_j, \mathbf{x}_k^{(i)}) + \dots + g_{12\dots p}(\mathbf{x}^{(i)}) \right)}{\partial x_j} \\ &= \frac{\partial g_j(x_j)}{\partial x_j} + \sum_{k=1}^{p-1} \sum_{\substack{W \subseteq -j, \\ |W|=k}} \frac{\partial g_{W \cup j}(\mathbf{x}_j, \mathbf{x}_W^{(i)})}{\partial x_j} \end{aligned}$$

Taking the conditional expectation over the local feature effects (partial derivatives) at x_j yields the (conditional) expected (i.e., global) feature effect at x_j :

$$\mathbb{E} \left[\frac{\partial \hat{f}(X_j, X_{-j})}{\partial x_j} \middle| X_j = x_j \right] = \frac{\partial g_j(x_j)}{\partial x_j} + \sum_{k=1}^{p-1} \sum_{\substack{W \subseteq -j, \\ |W|=k}} \mathbb{E} \left[\frac{\partial g_{W \cup j}(X_j, X_W)}{\partial x_j} \middle| X_j = x_j \right]$$

Based on these decompositions, we can show that the loss function for ALE only depends on the feature interaction effect between the j -th feature and features in $-j$ (Theorem 2):

$$\begin{aligned} \mathcal{L}^{ALE}(\mathcal{A}_g, x_j) &= \sum_{\substack{i: \mathbf{x}^{(i)} \in \mathcal{A}_g \wedge \\ \mathbf{x}^{(i)} \in \mathbb{P}(\mathbf{x}_{-j} | x_j)}} \left(\frac{\partial \hat{f}(x_j, \mathbf{x}_{-j}^{(i)})}{\partial x_j} - \mathbb{E} \left[\frac{\partial \hat{f}(X_j, X_{-j})}{\partial x_j} \middle| \mathcal{A}_g \wedge X_j = x_j \right] \right)^2 \\ &= \sum_{\substack{i: \mathbf{x}^{(i)} \in \mathcal{A}_g \wedge \\ \mathbf{x}^{(i)} \in \mathbb{P}(\mathbf{x}_{-j} | x_j)}} \left(\frac{\partial g_j(x_j)}{\partial x_j} + \sum_{k=1}^{p-1} \sum_{\substack{W \subseteq -j, \\ |W|=k}} \frac{\partial g_{W \cup j}(\mathbf{x}_j, \mathbf{x}_W^{(i)})}{\partial x_j} \right. \\ &\quad \left. - \frac{\partial g_j(x_j)}{\partial x_j} - \sum_{k=1}^{p-1} \sum_{\substack{W \subseteq -j, \\ |W|=k}} \mathbb{E} \left[\frac{\partial g_{W \cup j}(X_j, X_W)}{\partial x_j} \middle| \mathcal{A}_g \wedge X_j = x_j \right] \right)^2 \\ &= \sum_{\substack{i: \mathbf{x}^{(i)} \in \mathcal{A}_g \wedge \\ \mathbf{x}^{(i)} \in \mathbb{P}(\mathbf{x}_{-j} | x_j)}} \left(\sum_{k=1}^{p-1} \sum_{\substack{W \subseteq -j, \\ |W|=k}} \left(\frac{\partial g_{W \cup j}(\mathbf{x}_j, \mathbf{x}_W^{(i)})}{\partial x_j} - \mathbb{E} \left[\frac{\partial g_{W \cup j}(X_j, X_W)}{\partial x_j} \middle| \mathcal{A}_g \wedge X_j = x_j \right] \right) \right)^2 \end{aligned}$$

B.6 Applicability of SD Within GADGET

Here, we show the fulfillment of Axiom 1 defined in Section 4.2 for Shapley values, which are the underlying local feature effect in SD plots.

Local Decomposition: The local feature effect function in the SD plot is the Shapley value. We define $h(x_j, \mathbf{x}_{-j}^{(i)}) := \phi_j^{(i)}(x_j)$ to be the Shapley value for the i -th local feature effect at a fixed value x_j , which is typically the i -th feature value of \mathbf{x}_j (i.e., $x_j = \mathbf{x}_j^{(i)}$). In Eq. (8),

we defined $\phi_j^{(i)}(x_j)$ according to Herren and Hahn (2022) by the following decomposition:

$$\begin{aligned}\phi_j^{(i)}(x_j) &= \sum_{k=0}^{p-1} \frac{1}{k+1} \sum_{\substack{W \subseteq -j: \\ |W|=k}} \left(\mathbb{E}[\hat{f}(x_j, X_{-j}) | X_W = \mathbf{x}_W^{(i)}] - \sum_{V \subseteq \{W \cup j\}} \mathbb{E}[\hat{f}(X) | X_V = \mathbf{x}_V^{(i)}] \right) \\ &= g_j^c(x_j) + \sum_{k=1}^{p-1} \frac{1}{k+1} \sum_{W \subseteq -j: |W|=k} g_{W \cup j}^c(x_j, \mathbf{x}_W^{(i)}),\end{aligned}$$

with $g_{W \cup j}^c(x_j, \mathbf{x}_W^{(i)}) = \mathbb{E}[\hat{f}(x_j, X_{-j}) | X_W = \mathbf{x}_W^{(i)}] - \sum_{V \subseteq \{W \cup j\}} \mathbb{E}[\hat{f}(X) | X_V = \mathbf{x}_V^{(i)}]$. Hence, we can decompose h such that it only depends on main effects of and interaction effects with feature \mathbf{x}_j .

Taking the expectation over the local feature effects $h = \phi_j$ at x_j yields the expected (i.e., global) feature effect of Shapley values at $\mathbf{x}_j = x_j$.

$$\mathbb{E}_{X_W}[\phi_j(x_j)] = g_j^c(x_j) + \sum_{k=1}^{p-1} \frac{1}{k+1} \sum_{W \subseteq -j: |W|=k} \mathbb{E}[g_{W \cup j}^c(x_j, X_W)]$$

Based on these decompositions, we can show that the loss function for SD only depends on feature interactions between the j -th feature and features in $-j$ (Theorem 2):

$$\begin{aligned}\mathcal{L}^{SD}(\mathcal{A}_g, x_j) &= \sum_{i: \mathbf{x}^{(i)} \in \mathcal{A}_g \wedge \mathbf{x}_j^{(i)} = x_j} \left(\phi_j^{(i)}(x_j) - \mathbb{E}_{X_W}[\phi_j(x_j) | \mathcal{A}_g] \right)^2 \\ &= \sum_{i: \mathbf{x}^{(i)} \in \mathcal{A}_g \wedge \mathbf{x}_j^{(i)} = x_j} \left(g_j^c(x_j) + \sum_{k=1}^{p-1} \frac{1}{k+1} \sum_{W \subseteq -j: |W|=k} g_{W \cup j}^c(x_j, \mathbf{x}_W^{(i)}) \right. \\ &\quad \left. - g_j^c(x_j) + \sum_{k=1}^{p-1} \frac{1}{k+1} \sum_{W \subseteq -j: |W|=k} \mathbb{E}[g_{W \cup j}^c(x_j, X_W) | \mathcal{A}_g] \right)^2 \\ &= \sum_{i: \mathbf{x}^{(i)} \in \mathcal{A}_g \wedge \mathbf{x}_j^{(i)} = x_j} \left(\sum_{k=1}^{p-1} \frac{1}{k+1} \sum_{W \subseteq -j: |W|=k} \left(g_{W \cup j}^c(x_j, \mathbf{x}_W^{(i)}) - \mathbb{E}[g_{W \cup j}^c(x_j, X_W) | \mathcal{A}_g] \right) \right)^2\end{aligned}$$

Appendix C. Further Characteristics of Feature Effect Methods

In this section, we cover further characteristics of the different feature effect methods used within GADGET. As illustrated for PD in Section 4.3, we also show here for ALE and SD that the joint feature effect (and possibly the prediction function) within the final regions of GADGET can be approximated by the sum of univariate feature effects. Hence, the joint feature effect can be additively decomposed into the features' main effects within the final regions. Furthermore, we provide an overview on estimates and visualization techniques for the regional feature effects and interaction-related heterogeneity for the different feature effect methods. We also explain how categorical features are handled within GADGET, depending on the underlying feature effect method.

C.1 Decomposability of ALE

Figure 14 shows the effect plots when GADGET is applied to the uncorrelated simulation example of Section 3 when ALE (the underlying derivatives) and $S = Z = \{1, 2, 3\}$ are used. The grey curves before the split illustrate the global ALE curves. Since they do not show the interaction-related heterogeneity of the underlying local effects, we added a plot that visualizes this heterogeneity by providing the standard deviation of the derivatives within each interval as a (yellow) curve along the range of \mathbf{x}_j , similar to the idea of Goldstein et al. (2015) for derivative ICE curves. This shows us that local effects for feature \mathbf{x}_2 are very homogeneous over the entire range of \mathbf{x}_2 , while the local feature effects of \mathbf{x}_1 show a constant heterogeneous behavior and a regional high heterogeneity around $\mathbf{x}_3 = 0$ is visible for \mathbf{x}_3 . GADGET chooses $\mathbf{x}_3 = -0.003$ as the best split point that reduces the interaction-related heterogeneity of the three features almost completely. Thus, the ALE curves we receive in the subspaces are more representative for the underlying individuals.

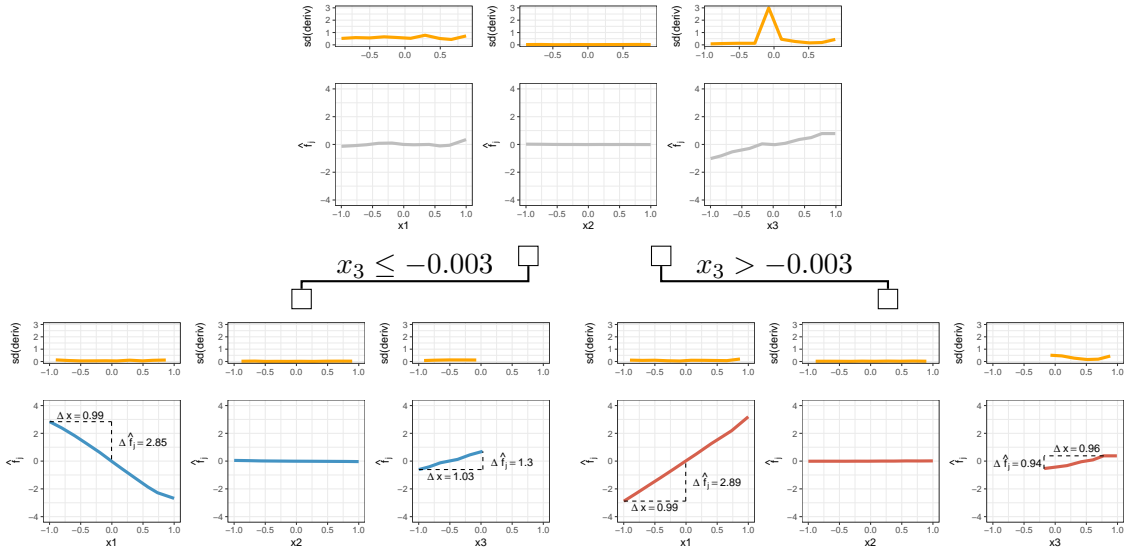


Figure 14: Visualization of applying GADGET with $S = Z = \{1, 2, 3\}$ to derivatives of ALE for the uncorrelated simulation example of Section 3 with $Y = 3X_1\mathbb{1}_{X_3>0} - 3X_1\mathbb{1}_{X_3\leq 0} + X_3 + \epsilon$ with $\epsilon \sim \mathcal{N}(0, 0.09)$. The upper plots show the standard deviation of the derivatives (yellow) and the ALE curves (grey) on the entire feature space, while the lower plots represent the respective standard deviation of the derivatives and regional ALE curves after partitioning the feature space w.r.t. $\mathbf{x}_3 = -0.003$.

Equivalently to PD plots, ALE plots also contain an additive recovery and, thus, can be decomposed additively in main and interaction effects (see Section 2.3). Furthermore, if Z is defined such that all features interacting with features in S are included and if GADGET is applied such that the theoretical minimum of the objective function is reached, then

according to Corollary 4, the joint mean-centered ALE function $f_{S|\mathcal{A}_g}^{ALE,c}$ within each final subspace \mathcal{A}_g can be decomposed into the 1-dimensional mean-centered ALE functions of features in S . Hence, since there are no more interactions between features in S and other features present in the final regions, $f_{S|\mathcal{A}_g}^{ALE,c}$ can be uniquely decomposed into the mean-centered main effects of features in S —just as in PD functions (Apley and Zhu, 2020):

$$f_{S|\mathcal{A}_g}^{ALE,c}(\mathbf{x}_S) = \sum_{j \in S} f_{j|\mathcal{A}_g}^{ALE,c}(\mathbf{x}_j) \quad (18)$$

Moreover, let $-S$ be the subset of features that do not interact with any other features. Then, according to Eq. (18) and Eq. (4), the prediction function $\hat{f}_{\mathcal{A}_g}$ within the region \mathcal{A}_g can be decomposed into the 1-dimensional mean-centered ALE functions of all p features, plus some constant value g_0 :

$$\hat{f}_{\mathcal{A}_g}(\mathbf{x}) = g_0 + \sum_{j=1}^p f_{j|\mathcal{A}_g}^{ALE,c}(\mathbf{x}_j).$$

We can again derive this decomposition from Figure 14, where \mathbf{x}_2 shows an effect of 0 with low heterogeneity before and after the split. The feature effects of \mathbf{x}_1 and \mathbf{x}_3 show high heterogeneity before the split, which is almost completely minimized after the split w.r.t. \mathbf{x}_3 . Hence, the resulting regional (linear) ALE curves are representative estimates for the underlying local effects. Therefore, we can approximate the prediction function within each subspace by

$$\hat{f}_{\mathcal{A}_l}(\mathbf{x}) = g_0 + \frac{-2.85}{0.99}\mathbf{x}_1 + \frac{1.3}{1.03}\mathbf{x}_3 = g_0 - 2.89\mathbf{x}_1 + 1.26\mathbf{x}_3$$

and

$$\hat{f}_{\mathcal{A}_r}(\mathbf{x}) = g_0 + \frac{2.89}{0.99}\mathbf{x}_1 + \frac{0.94}{0.96}\mathbf{x}_3 = g_0 + 2.92\mathbf{x}_1 + 0.98\mathbf{x}_3.$$

Particularities of ALE Estimation. As seen for the continuous feature \mathbf{x}_3 in the simulation example presented here, abrupt interactions (“jumps”)²² might be difficult to estimate for models that learn smooth effects, such as NNs (used here) or SVMs—especially when compared to models such as decision trees. Hence, depending on the model, these type of feature interactions can lead to very high partial derivatives in a region around the “jump” point instead of a high partial derivative at exactly the one specific “jump” point (here: $\mathbf{x}_3 = 0$), thus leading to non-reducible heterogeneity. This is illustrated in the upper right plot of Figure 14. The standard deviation of the derivatives of \mathbf{x}_3 are very high in the region around and not exactly at $\mathbf{x}_3 = 0$. This interaction-related heterogeneity should be (almost) completely reduced when splitting w.r.t. $\mathbf{x}_3 = 0$. However, high values will remain, since the model did not perfectly capture this kind of interaction. To account for this issue in the estimation and partitioning process within GADGET, we use the following procedure for continuous features: In the two new subspaces after a split, if the derivatives of feature values close to the split point vary at least twice as much (measured by the

22. With abrupt interaction, we mean interactions that lead to an abrupt change of the influence of one feature (\mathbf{x}_1) based on the influence of another feature at a specific (“jump”) point ($\mathbf{x}_3 = 0$) like the feature interaction between \mathbf{x}_1 and \mathbf{x}_3 in the here presented simulation example: $Y = 3X_1\mathbb{1}_{X_3>0} - 3X_1\mathbb{1}_{X_3\leq 0} + X_3 + \epsilon$ with $\epsilon \sim \mathbb{N}(0, 0.09)$.

standard deviation) as the derivatives of the other observations within each subspace, then the derivatives of feature values close to the split point are replaced by values drawn from a normally distributed random variable where mean and variance are estimated by the derivatives of the remaining observation within each subspace.

C.2 Decomposability of SD

Recalculation Versus No Recalculation of Shapley Values. In Section 4.5, we argued that Shapley values must be recalculated after each partitioning step in order for each new subspace to receive SD effects in the final subspaces that are representative of the underlying main effects within each subspace. Meanwhile, the unconditional expected value (i.e., the feature interactions on the entire feature space) are minimized without recalculating the conditional expected values.

The difference in the final feature effects within the subspaces is illustrated when comparing the left plot of Figure 5 (split without recalculation) with the respective plots of feature \mathbf{x}_1 of Figure 15. Without recalculation, the effect of feature \mathbf{x}_1 is still regarded as an interaction effect between \mathbf{x}_1 and \mathbf{x}_3 , and hence only half of the joint interaction effect is assigned to \mathbf{x}_1 (i.e., the respective slope within the regions is 1.5 and -1.5 instead of 3 and -3), and the other half of the joint interaction effect is assigned to \mathbf{x}_3 . When Shapley values are recalculated after the first partitioning step within each subspace, we can see in Figure 15 that no more interactions are present between \mathbf{x}_1 and \mathbf{x}_3 within each subspace, due to the split w.r.t. \mathbf{x}_3 . Hence, the effect of \mathbf{x}_1 is recognized as the main effect with the slope approximately defined in the data-generating process. Furthermore, due to interactions with \mathbf{x}_1 , the heterogeneity of feature effects of \mathbf{x}_3 is also reduced after the split, owing to recalculation.

Note: If the feature we use for partitioning the feature space ($z \in Z$) coincides with the features of interest (S), then the Shapley values should be recalculated in Algorithm 1 to find the best split point (at least, if we choose the approach with recalculation after each partitioning step). The reason is that if $z \in S$, we also want to reduce the interaction-related heterogeneity within z that is not accounted for if we do not recalculate the Shapley values within the new subspace. For example, in Figure 15, we split according to \mathbf{x}_3 , which is also a feature of interest ($3 \in S$). If we do not recalculate the Shapley values for \mathbf{x}_3 within the splitting process, then the sum of the risk of any two subspaces for \mathbf{x}_3 will always be approximately the same as the risk of the parent node, and thus the heterogeneity reduction for \mathbf{x}_3 (which is shown in the regional plots of Figure 15) is not considered in the objective of Algorithm 1.

Decomposition. Herren and Hahn (2022) show that Shapley values can be decomposed by weighted PD functions (see Eq. 8)). Hence, if the global SD feature effect as defined in Eq. (16) is considered, the same decomposition rules as defined for PD plots apply. In other words, if Z contains all features that interact with features in S and if GADGET is applied such that the theoretical minimum of the objective function is reached, then according to Corollary 4, the following decomposition in 1-dimensional global SD effect functions of features in S holds:

$$f_{S|\mathcal{A}_g}^{SD}(\mathbf{x}_S) = \sum_{j \in S} f_{j|\mathcal{A}_g}^{SD}(\mathbf{x}_j). \quad (19)$$

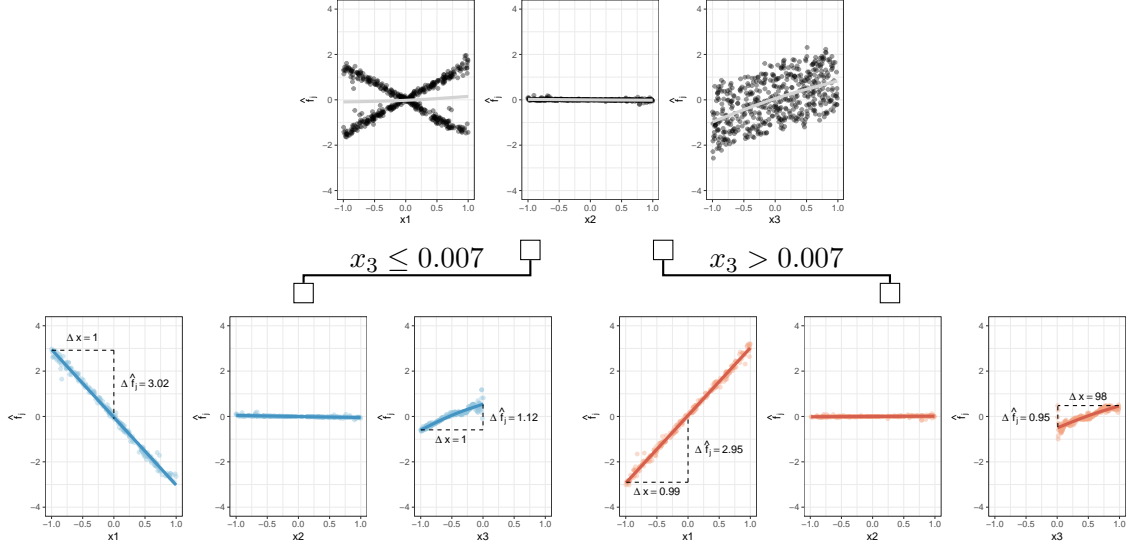


Figure 15: Visualization of applying GADGET with $S = Z = \{1, 2, 3\}$ to Shapley values of the uncorrelated simulation example of Section 3 with $Y = 3X_1 \mathbb{1}_{X_3 > 0} - 3X_1 \mathbb{1}_{X_3 \leq 0} + X_3 + \epsilon$ with $\epsilon \sim \mathcal{N}(0, 0.09)$. The upper plots show the Shapley values and the global estimated SD curve on the entire feature space, while the lower plots represent the respective Shapley values and regional SD curves after partitioning the feature space w.r.t. $\mathbf{x}_3 = 0.007$.

If all features containing heterogeneous effects (feature interactions) are included in the subset S , and the subset Z consists of all features that interact with features in S , then according to Eq. (19) and Eq. (4), the prediction function $\hat{f}_{\mathcal{A}_g}$ within the region \mathcal{A}_g can be uniquely decomposed into the 1-dimensional global SD effect functions of all p features, plus some constant value g_0 :

$$\hat{f}_{\mathcal{A}_g}(\mathbf{x}) = g_0 + \sum_{j=1}^p f_{j|\mathcal{A}_g}^{SD}(\mathbf{x}_j).$$

Again, we can derive this decomposition from Figure 14 in the same way we did for PD and ALE plots. Hence, we can approximate the prediction function within each subspace by $\hat{f}_{\mathcal{A}_l}(\mathbf{x}) = g_0 - 3.02\mathbf{x}_1 + 1.12\mathbf{x}_3$ and $\hat{f}_{\mathcal{A}_r}(\mathbf{x}) = g_0 + 2.98\mathbf{x}_1 + 1.03\mathbf{x}_3$.

Equivalence of SD and Mean-Centered PD. According to Herren and Hahn (2022), the Shapley value $\phi_j^{(i)}(x_j)$ of the i -th observation at $\mathbf{x}_j = x_j$ can be decomposed as defined in

Eq. (8) to

$$\begin{aligned}\phi_j^{(i)}(x_j) &= \sum_{k=0}^{p-1} \frac{1}{k+1} \sum_{\substack{W \subseteq -j: \\ |W|=k}} \left(\mathbb{E}[\hat{f}(x_j, X_{-j}) | X_W = \mathbf{x}_W^{(i)}] - \sum_{V \subset \{W \cup j\}} \mathbb{E}[\hat{f}(X) | X_V = \mathbf{x}_V^{(i)}] \right) \\ &= g_j^c(x_j) + \sum_{k=1}^{p-1} \frac{1}{k+1} \sum_{W \subseteq -j: |W|=k} g_{W \cup j}^c(x_j, \mathbf{x}_W^{(i)}),\end{aligned}$$

with $g_{W \cup j}^c(x_j, \mathbf{x}_W^{(i)}) = \mathbb{E}[\hat{f}(x_j, X_{-j}) | X_W = \mathbf{x}_W^{(i)}] - \sum_{V \subset \{W \cup j\}} \mathbb{E}[\hat{f}(X) | X_V = \mathbf{x}_V^{(i)}]$.

As in Eq. (16), the global feature effect (SD) of feature \mathbf{x}_j at x_j is then defined by

$$f_j^{SD}(x_j) = \mathbb{E}_{X_W}[\phi_j] = g_j^c(x_j) + \sum_{k=1}^{p-1} \frac{1}{k+1} \sum_{W \subseteq -j: |W|=k} \mathbb{E}[g_{W \cup j}^c(x_j, X_W)]$$

Hence, if Corollary 4 is satisfied, if the joint global SD effect of features in S can be decomposed into the univariate SD effects as in Eq. (19), and if the interventional approach for Shapley calculation is used, then all feature interactions are zero, and the global SD effect of feature \mathbf{x}_j at x_j is given by

$$\begin{aligned}f_j^{Shap}(x_j) &= g_j^c(x_j) + \sum_{k=1}^{p-1} \frac{1}{k+1} \sum_{W \subseteq -j: |W|=k} \mathbb{E}[g_{W \cup j}^c(x_j, X_W)] \\ &\stackrel{\text{Cor. 4}}{=} g_j^c(x_j) \\ &= \mathbb{E}[\hat{f}(x_j, X_{-j})] - \mathbb{E}[\hat{f}(X)],\end{aligned}$$

which is equivalent to the mean-centered PD of feature \mathbf{x}_j at x_j .

C.3 Overview on Estimates and Visualizations

We provide here an overview on the estimates and visualization techniques for PD, ALE, and SD within GADGET that we introduced in Sections 4.3-4.5.

Local Effect. The local effect h for a feature \mathbf{x}_j at feature value x_j used within GADGET is estimated by

- **PD:** mean-centered ICE $\hat{h}^{(i)} = \hat{f}^c(x_j, \mathbf{x}_{-j}^{(i)})$
- **ALE:** partial derivatives estimated by prediction differences within k -th interval $\hat{h}^{(i)} = \hat{f}(z_{k-1,j}, \mathbf{x}_{-j}^{(i)}) - \hat{f}(z_{k-1,j}, \mathbf{x}_{-j}^{(i)})$ where $x_j \in]z_{k-1,j}, z_{k,j}]$
- **SD:** Shapley value $\hat{h}^{(i)} = \hat{\phi}_j^{(i)}$

Regional Effect. The feature effect for a feature \mathbf{x}_j at feature value x_j within a subspace/region \mathcal{A}_g of GADGET is estimated by

- **PD:** mean-centered regional PD $\hat{f}_{j|\mathcal{A}_g}^{PD,c}(x_j) = \frac{1}{|N_g|} \sum_{i \in N_g} \hat{f}^c(x_j, \mathbf{x}_{-j}^{(i)})$ with N_g being the index set of all $i : \mathbf{x}^{(i)} \in \mathcal{A}_g$.
- **ALE:** regional ALE $\hat{f}_{j|\mathcal{A}_g}^{ALE}(x_j) = \sum_{k=1}^{k_j(x_j)} \frac{1}{|N_g(k)|} \sum_{i \in N_g(k)} [\hat{f}(z_{k,j}, \mathbf{x}_{-j}^{(i)}) - \hat{f}(z_{k-1,j}, \mathbf{x}_{-j}^{(i)})]$ with $N_g(k)$ being the index set of all $i : x_j \in]z_{k-1,j}, z_{k,j}] \wedge \mathbf{x}^{(i)} \in \mathcal{A}_g$.
- **SD:** regional SD $\hat{f}_{j|\mathcal{A}_g}^{SD}(x_j)$ is estimated by fitting a GAM on $\{\mathbf{x}_j^{(i)}, \hat{\phi}_j^{(i)}\}_{i:\mathbf{x}^{(i)} \in \mathcal{A}_g}$.

The regional effect for feature \mathbf{x}_j is visualized for all $x_j \in \mathcal{A}_g$. Therefore, the respective GAM curve is plotted in the case of SD, while we linearly interpolate between the grid-wise/interval-wise estimates of PD/ALE to receive the regional effect curves.

Interaction-Related Heterogeneity. The interaction-related heterogeneity for a feature \mathbf{x}_j at feature value x_j within a subspace/region \mathcal{A}_g of GADGET is estimated by the loss function in Eq. (10), which quantifies the variance of local effects at x_j and is visualized by

- **PD:** 95% interval around (mean-centered) regional PD estimate $[\hat{f}_{j|\mathcal{A}_g}^{PD,c}(x_j) \pm 1.96 \cdot \sqrt{\hat{\mathcal{L}}^{PD}(\mathcal{A}_g, x_j)}]$.
- **ALE:** standard deviation of local effects $\sqrt{\hat{\mathcal{L}}^{ALE}(\mathcal{A}_g, x_j)}$.
- **SD:** Shapley values are recalculated within each region \mathcal{A}_g and plotted with the fitted GAM for the regional SD effect to visualize the variation of local feature effects aka interaction-related heterogeneity.

For each feature $j \in S$, we generate one figure showing the regional effect curves of all final regions we obtain after applying GADGET. For PD, the regional effect curves are accompanied with intervals showing how much interaction-related heterogeneity remains in the underlying local effects (see, e.g., Figures 11). For ALE, a separate plot visualizes the interaction-related heterogeneity via the standard deviation of local effects, which is inspired by the derivative ICE plots of Goldstein et al. (2015) (see, e.g., Figure 12). For SD, the Shapley values that were recalculated conditioned on each subspace \mathcal{A}_g are visualized with the regional effect curve (see, e.g., Figure 18).

Note that we can also visualize the non-centered PD ($\hat{f}_{j|\mathcal{A}_g}^{PD}$) instead of the mean-centered PD, which might provide more insights regarding interpretation. However, the interaction-related heterogeneity must be estimated by the mean-centered ICE curves to only represent heterogeneity induced by feature interactions (see Appendix B.4).

C.4 Handling of Categorical Features

In this section, we will summarize the particularities of categorical features. Compared to numeric features, we have a limited number of K values (categories). Hence, compared to numeric features, we find split points by dividing the K categories into the two new

subspaces. Since GADGET is based on the general concept of a CART (decision tree) algorithm (Breiman et al., 1984) that can handle categorical features, the splitting itself follows the same approach as for a common CART algorithm. If we have categorical features in S , it does influence the calculation of our objective function, and the handling depends on the underlying feature effect method. We briefly discuss the specifics for each of the three feature effect methods that we use in this paper. All of them are able to handle categorical features, which is a general requirement that we can use it for mixed data sets within GADGET.

PD Plot. Compared to numeric features, the grid points for categorical features are limited to the number of categories. Otherwise, the calculation of the loss and the risk (see, Eq. 13 and Eq. 11) works exactly the same as for numeric features.²³

ALE Plot. ALE builds intervals based on quantiles for numeric features to calculate prediction differences between neighboring interval borders for all observations falling within this interval. For binary features, the authors solve this as follows: for all observations falling in each of the categories, the prediction difference when changing it to the other category is calculated. For more categories, they suggest a sorting algorithm.²⁴ Hence, we still receive the needed derivatives for GADGET for each category to calculate the loss and risk function for GADGET.

SD Plot. Compared to numeric features, the x-axis of the SD plot is a grid of size K . For each of these grid points (categories), the Shapley values for the observations belonging to the specific category are calculated. Hence, instead of a spline to quantify the expected value in Eq. (17), we use the arithmetic mean within each category (similar to PD plots) and, thus, sum up the variance of Shapley values for each category over all categories (within the respective subspace).

In general, if we apply GADGET and split w.r.t. a categorical feature such that only one category is present within a subspace (e.g., we split the feature sex such that all individuals are male in one resulting subspace), then the interaction related heterogeneity vanishes to zero, since only an additive shift for the feature sex is left in this subspace.

Note: If a categorical feature \mathbf{x}_j is not only considered for splitting ($j \in Z$) but is also a feature of interest ($j \in S$), the different splitting possibilities of categories of \mathbf{x}_j prompt recalculation for ALE, since derivatives are only calculated for pre-sorted neighboring categories. In our implementations, we only split w.r.t. the pre-sorted categories and considered them as integer values to reduce the computational burden of the calculations.

Appendix D. Additions to PINT

Although the approximation of the null distribution via theoretical distributions reduces the computational burden when applying PINT (as described in Section 5), it is still high for high-dimensional settings. Therefore, we suggest to randomly select a smaller set of observations to apply PINT in the case of a high number of observations. In the case of

23. Since we calculate the loss point-wise at each grid point and sum it up over all grid points, the order of the category does not make a difference for the objective of GADGET.

24. For more information, we refer to Apley and Zhu (2020).

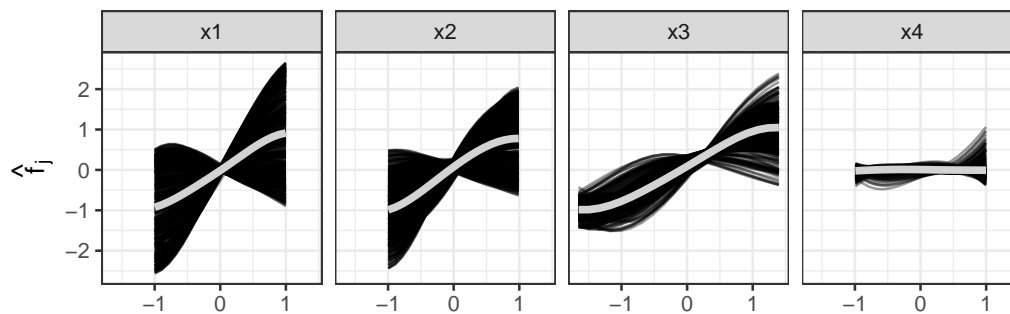


Figure 16: Mean-centered ice curves (black) and mean-centered PD curves (grey) for all four features of one repetition of the simulation example described in Section 5.

many features, we recommend to filter features beforehand and apply PINT only once to those with the highest possibility of containing feature interactions. For example, this can be done by excluding features that show only small variations of the local feature effects used in GADGET, since the homogeneous feature effects are a strong indicator that the feature does not interact with any other feature. For instance, the mean-centered ICE curves of \mathbf{x}_4 in Figure 16 show only small variation, which indicates that \mathbf{x}_4 does not interact with any other feature, and thus there is no need to consider it for PINT. Hence, we can apply PINT only on the remaining three features to identify which features interact with each other and must be considered within GADGET.

Appendix E. Further Details on Real-World Applications

COMPAS Data Set. Our analysis in Section 7 for the COMPAS data set is based on a tuned SVM. We chose this model based on the following selection process: For the binary classification task²⁵, we chose to select the best model out of a logistic regression, a random forest, and a tuned SVM with RBF kernel. We also compared these models to a featureless model. The model selection was performed by a 5-fold cross-validation, where the hyperparameters cost C and inverse kernel width σ of the SVM were tuned via 3-fold cross-validation on the inner folds of the nested resampling approach.²⁶ We evaluate the learners’ test performance on the outer folds based on the F1 score and Matthews correlation coefficient (MCC) (Chicco and Jurman, 2020). Since the tuned SVM performs best w.r.t. both evaluation metrics, we chose this model for our further analysis. Note that the performance differences between the different learners (besides the featureless baseline) are very small. Thus, one might consider using the most interpretable learner (here, logistic regression) for further analysis. However, since the purpose of our analysis is to detect feature

25. The classes are slightly unbalanced, with 1317 defendants who have a high risk of recidivism and 2056 defendants with a low risk of recidivism.

26. For tuning, we used random search with 30 iterations on a search space of 2^{-12} to 2^{12} for each of the two hyperparameters.

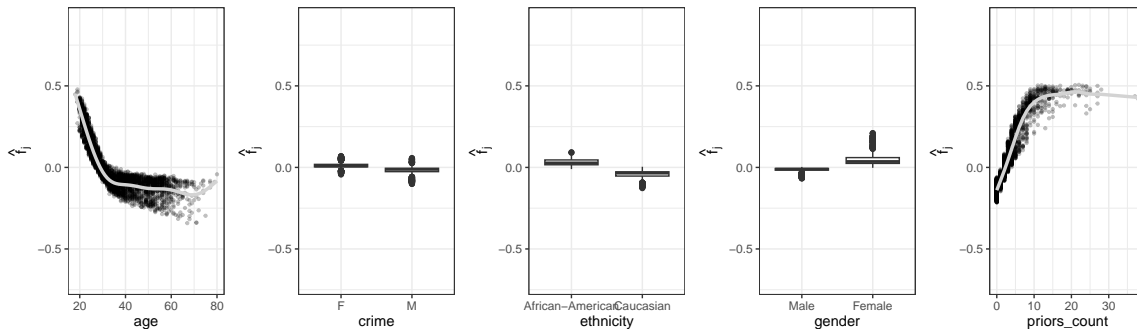


Figure 17: Global SD curves and Shapley values of considered features of the COMPAS application example.

interactions and reduce interaction-related heterogeneity by partitioning the feature space, here we choose the best-performing model that also potentially learned feature interactions.

Learner	MCC	F1 Score
Featureless	0.0000	0.7573
Logistic Regression	0.4675	0.8057
Random Forest	0.4710	0.8125
Support Vector Machine (tuned)	0.4752	0.8126

Table 6: Average learner test performance on 5-fold cross-validation for COMPAS data set.

In addition to the results of GADGET based on PD presented in Section 7, we also applied GADGET with the same settings based on SD.

The effect plots for the four resulting regions are shown in Figure 18. GADGET based on SD performs the same first split as for PD. The second split is also executed according to the number of prior crimes, but the split value is lower than for PD (at 2.5 instead of 4.5). The total interaction-related heterogeneity reduction ($R_{Tot}^2 = 0.87$) is also similar to that when PD is used. Note that Shapley values explain the difference between the the actual and average prediction. Hence, SD plots are centered, while Figure 11 shows the uncentered regional PD plots.

Bikesharing Data Set. The results in Section 7 for the Bikesharing data set are based on a random forest. We chose this model based on the following selection process: For the underlying regression task, we selected the best-performing model out of a linear model, a random forest, and a tuned SVM with RBF kernel. As a baseline comparison, we also report the performance of a featureless model. The model selection was performed by a 5-fold cross-validation, where the hyperparameters cost C and inverse kernel width σ of the SVM were tuned via 3-fold cross-validation on the inner folds of the nested resampling

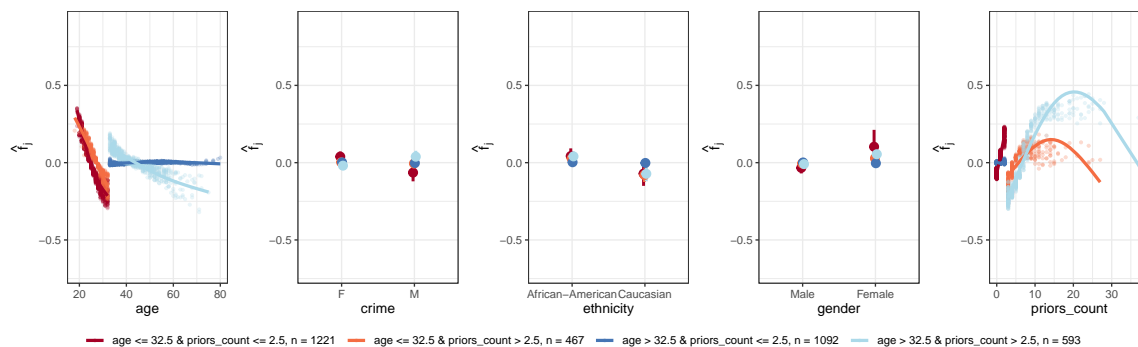


Figure 18: Regional SD plots for considered features of the COMPAS application after applying GADGET. Shapley values within each region are recalculated and visualize the interaction-related heterogeneity within each region.

approach.²⁷ We evaluate the learners’ test performance on the outer folds based on the MSE and an R^2 . The random forest performed best and, hence, was chosen for further analyses.

Learner	MSE	R^2
Featureless	17902	-0.0002
Linear Regression	6641	0.6289
Random Forest	1077	0.9397
Support Vector Machine (tuned)	3365	0.8114

Table 7: Average learner test performance on 5-fold cross-validation for bikesharing data set.

References

Kjersti Aas, Martin Jullum, and Anders Løland. Explaining individual predictions when features are dependent: More accurate approximations to Shapley values. *Artificial Intelligence*, 298:103502, September 2021.

André Altmann, Laura Toloşi, Oliver Sander, and Thomas Lengauer. Permutation importance: a corrected feature importance measure. *Bioinformatics*, 26(10):1340–1347, 04 2010.

Daniel W. Apley and Jingyu Zhu. Visualizing the effects of predictor variables in black box supervised learning models. *Journal of the Royal Statistical Society: Series B (Statistical Methodology)*, 82(4):1059–1086, 2020.

²⁷. For tuning, we used random search with 30 iterations on a search space of 2^{-12} to 2^{12} for each of the two hyperparameters.

- Irene V Blair, Charles M Judd, and Kristine M Chapleau. The influence of afrocentric facial features in criminal sentencing. *Psychological science*, 15(10):674–679, 2004.
- Stefan Blücher, Johanna Vielhaben, and Nils Strodthoff. Preddiff: Explanations and interactions from conditional expectations. *Artificial Intelligence*, 312:103774, November 2022.
- Sebastian Bordt and Ulrike von Luxburg. From Shapley values to generalized additive models and back. In *International Conference on Artificial Intelligence and Statistics*, pages 709–745. PMLR, 2023.
- Leo Breiman, J. H. Friedman, R. A. Olshen, and C. J. Stone. *Classification and Regression Trees*. Wadsworth, 1984.
- Matthew Britton. Vine: Visualizing statistical interactions in black box models. *arXiv preprint arXiv:1904.00561*, 2019.
- Siu Lun Chau, Robert Hu, Javier Gonzalez, and Dino Sejdinovic. Rkhs-shap: Shapley values for kernel methods. In *Advances in Neural Information Processing Systems*, volume 35, pages 13050–13063, 2022.
- Hugh Chen, Joseph D. Janizek, Scott Lundberg, and Su-In Lee. True to the model or true to the data? *arXiv preprint arXiv:2006.16234*, 2020.
- Davide Chicco and Giuseppe Jurman. The advantages of the Matthews correlation coefficient (mcc) over f1 score and accuracy in binary classification evaluation. *BMC genomics*, 21:1–13, 2020.
- Aaron Fisher, Cynthia Rudin, and Francesca Dominici. All models are wrong, but many are useful: Learning a variable’s importance by studying an entire class of prediction models simultaneously. *Journal of Machine Learning Research*, 20(177):1–81, 2019.
- Jerome H. Friedman. Greedy function approximation: A gradient boosting machine. *The Annals of Statistics*, 29(5):1189–1232, 2001.
- Jerome H. Friedman and Bogdan E. Popescu. Predictive learning via rule ensembles. *The Annals of Applied Statistics*, 2(3):916–954, 2008.
- Alex Goldstein, Adam Kapelner, Justin Bleich, and Emil Pitkin. Peeking inside the black box: Visualizing statistical learning with plots of individual conditional expectation. *Journal of Computational and Graphical Statistics*, 24(1):44–65, January 2015.
- Brandon M. Greenwell, Bradley C. Boehmke, and Andrew J. McCarthy. A simple and effective model-based variable importance measure. *arXiv preprint arXiv:1805.04755*, 2018.
- Julia Herbinge, Bernd Bischl, and Giuseppe Casalicchio. Repid: Regional effect plots with implicit interaction detection. In *International Conference on Artificial Intelligence and Statistics*, pages 10209–10233. PMLR, 2022.

- Andrew Herren and P. Richard Hahn. Statistical aspects of shap: Functional anova for model interpretation. *arXiv preprint arXiv:2208.09970*, 2022.
- Munir Hiabu, Joseph T Meyer, and Marvin N Wright. Unifying local and global model explanations by functional decomposition of low dimensional structures. In *International Conference on Artificial Intelligence and Statistics*, pages 7040–7060. PMLR, 2023.
- Giles Hooker. Discovering additive structure in black box functions. In *Proceedings of the tenth ACM SIGKDD International Conference on Knowledge Discovery and Data mining*, pages 575–580, 2004.
- Giles Hooker. Generalized functional anova diagnostics for high-dimensional functions of dependent variables. *Journal of Computational and Graphical Statistics*, 16(3):709–732, September 2007.
- Linwei Hu, Jie Chen, Vijayan N Nair, and Agus Sudjianto. Surrogate locally-interpretable models with supervised machine learning algorithms. *arXiv preprint arXiv:2007.14528*, 2020.
- Linwei Hu, Jie Chen, and Vijayan N. Nair. Using model-based trees with boosting to fit low-order functional anova models. *arXiv preprint arXiv:2207.06950*, 2022.
- Alan Inglis, Andrew Parnell, and Catherine B. Hurley. Visualizing variable importance and variable interaction effects in machine learning models. *Journal of Computational and Graphical Statistics*, 31(3):766–778, July 2022.
- Gareth James, Daniela Witten, Trevor Hastie, and Rob Tibshirani. *ISLR2: Introduction to Statistical Learning, Second Edition*, 2022. R package version 1.3-2.
- Neil Jethani, Mukund Sudarshan, Ian Connick Covert, Su-In Lee, and Rajesh Ranganath. Fastshap: Real-time Shapley value estimation. In *International Conference on Learning Representations*, 2021.
- Indra Kumar, Carlos Scheidegger, Suresh Venkatasubramanian, and Sorelle Friedler. Shapley residuals: Quantifying the limits of the Shapley value for explanations. In *Advances in Neural Information Processing Systems*, volume 34, pages 26598–26608, 2021.
- Jeff Larson, Surya Mattu, Lauren Kirchner, and Julia Angwin. How we analyzed the compas recidivism algorithm. *ProPublica*, 2016. URL <https://www.propublica.org/article/how-we-analyzed-the-compas-recidivism-algorithm>.
- Benjamin Lengerich, Sarah Tan, Chun-Hao Chang, Giles Hooker, and Rich Caruana. Purifying interaction effects with the functional anova: An efficient algorithm for recovering identifiable additive models. In *International Conference on Artificial Intelligence and Statistics*, pages 2402–2412. PMLR, 2020.
- Genyuan Li and Herschel Rabitz. General formulation of hdmr component functions with independent and correlated variables. *Journal of Mathematical Chemistry*, 50(1):99–130, January 2012.

- Zachary C Lipton. The mythos of model interpretability: In machine learning, the concept of interpretability is both important and slippery. *Queue*, 16(3):31–57, 2018.
- Scott M Lundberg and Su-In Lee. A unified approach to interpreting model predictions. In *Advances in Neural Information Processing Systems*, volume 30, 2017.
- Scott M. Lundberg, Gabriel G. Erion, and Su-In Lee. Consistent individualized feature attribution for tree ensembles. *arXiv preprint arXiv:1802.03888*, March 2019.
- Scott M Lundberg, Gabriel Erion, Hugh Chen, Alex DeGrave, Jordan M Prutkin, Bala Nair, Ronit Katz, Jonathan Himmelfarb, Nisha Bansal, and Su-In Lee. From local explanations to global understanding with explainable ai for trees. *Nature machine intelligence*, 2(1): 56–67, 2020.
- Aria Masoomi, Davin Hill, Zhonghui Xu, Craig P Hersh, Edwin K Silverman, Peter J Castaldi, Stratis Ioannidis, and Jennifer Dy. Explanations of black-box models based on directional feature interactions. *arXiv preprint arXiv:2304.07670*, 2023.
- Ninareh Mehrabi, Fred Morstatter, Nripsuta Saxena, Kristina Lerman, and Aram Galstyan. A survey on bias and fairness in machine learning. *ACM Computing Surveys (CSUR)*, 54(6):1–35, 2021.
- Christoph Molnar. *Interpretable Machine Learning*. 2 edition, 2022. URL <https://christophm.github.io/interpretable-ml-book>.
- Christoph Molnar, Gunnar König, Julia Herbinger, Timo Freiesleben, Susanne Dandl, Christian A Scholbeck, Giuseppe Casalicchio, Moritz Grosse-Wentrup, and Bernd Bischl. General pitfalls of model-agnostic interpretation methods for machine learning models. In *xxAI-Beyond Explainable AI: International Workshop, Held in Conjunction with ICML 2020, July 18, 2020, Vienna, Austria, Revised and Extended Papers*, pages 39–68. Springer, 2022.
- Christoph Molnar, Gunnar König, Bernd Bischl, and Giuseppe Casalicchio. Model-agnostic feature importance and effects with dependent features: a conditional subgroup approach. *Data Mining and Knowledge Discovery*, pages 1–39, 2023.
- Sharif Rahman. A generalized anova dimensional decomposition for dependent probability measures. *SIAM/ASA Journal on Uncertainty Quantification*, 2:670–697, January 2014.
- Christian A Scholbeck, Giuseppe Casalicchio, Christoph Molnar, Bernd Bischl, and Christian Heumann. Marginal effects for non-linear prediction functions. *arXiv preprint arXiv:2201.08837*, 2022.
- Lloyd S Shapley. A value for n-person games. *Contributions to the Theory of Games*, 2(28): 307–317, 1953.
- Margaret A Shipp, Ken N Ross, Pablo Tamayo, Andrew P Weng, Jeffery L Kutok, Ricardo CT Aguiar, Michelle Gaasenbeek, Michael Angelo, Michael Reich, Geraldine S Pinkus, et al. Diffuse large b-cell lymphoma outcome prediction by gene-expression profiling and supervised machine learning. *Nature medicine*, 8(1):68–74, 2002.

- Daria Sorokina, Rich Caruana, Mirek Riedewald, and Daniel Fink. Detecting statistical interactions with additive groves of trees. In *Proceedings of the 25th International Conference on Machine Learning*, pages 1000–1007, 2008.
- Clemens Stachl, Florian Pargent, Sven Hilbert, Gabriella M Harari, Ramona Schoedel, Sumer Vaid, Samuel D Gosling, and Markus Bühner. Personality research and assessment in the era of machine learning. *European Journal of Personality*, 34(5):613–631, 2020.
- Charles J. Stone. The use of polynomial splines and their tensor products in multivariate function estimation. *The Annals of Statistics*, 22(1):118 – 171, 1994.
- Erik Štrumbelj and Igor Kononenko. Explaining prediction models and individual predictions with feature contributions. *Knowledge and Information Systems*, 41:647–665, 2014.
- Xingzhi Sun, Ziyu Wang, Rui Ding, Shi Han, and Dongmei Zhang. Puregam: Learning an inherently pure additive model. In *Proceedings of the 28th ACM SIGKDD Conference on Knowledge Discovery and Data Mining*, pages 1728–1738, 2022.
- Mukund Sundararajan and Amir Najmi. The many Shapley values for model explanation. In *Proceedings of the 37th International Conference on Machine Learning*, pages 9269–9278, 2020.
- Sarah Tan, Giles Hooker, Paul Koch, Albert Gordo, and Rich Caruana. Considerations when learning additive explanations for black-box models. *arXiv preprint arXiv:1801.08640*, 2018.
- Che-Ping Tsai, Chih-Kuan Yeh, and Pradeep Ravikumar. Faith-shap: The faithful Shapley interaction index. *Journal of Machine Learning Research*, 24(94):1–42, 2023.
- Xiaohang Zhang, Yuan Wang, and Zhengren Li. Interpreting the black box of supervised learning models: Visualizing the impacts of features on prediction. *Applied Intelligence*, 51(10):7151–7165, October 2021.